



HAL
open science

Extended stress gradient elastodynamics: Wave dispersion and micro-macro identification of parameter

Logan Schwan, Nicolas Favrie, Régis Cottureau, Bruno Lombard

► **To cite this version:**

Logan Schwan, Nicolas Favrie, Régis Cottureau, Bruno Lombard. Extended stress gradient elastodynamics: Wave dispersion and micro-macro identification of parameter. *International Journal of Solids and Structures*, 2021, 219-220, pp.34-50. hal-02909331

HAL Id: hal-02909331

<https://hal.science/hal-02909331>

Submitted on 30 Jul 2020

HAL is a multi-disciplinary open access archive for the deposit and dissemination of scientific research documents, whether they are published or not. The documents may come from teaching and research institutions in France or abroad, or from public or private research centers.

L'archive ouverte pluridisciplinaire **HAL**, est destinée au dépôt et à la diffusion de documents scientifiques de niveau recherche, publiés ou non, émanant des établissements d'enseignement et de recherche français ou étrangers, des laboratoires publics ou privés.

8 *Keywords:* Stress gradient media Generalized continua, Second-order
9 homogenization, Wave dispersion, Hyperbolic system
10 *2000 MSC:* code, code

11 **1. Introduction**

12 Over the past decades, many extensions to the classical continuum me-
13 chanics theory have emerged [1], such as micro-polar [2] or more general
14 micro-continuum mechanics theories [3, 4, 5]. As alternative approaches
15 to atomistic models for micro-structured media, such extended continuum
16 models have been developed to incorporate physical phenomena involving
17 size effects beyond the reach of the classical theories. While many extended
18 continuum models were developed in statics [6, 7], microstructural size ef-
19 fects are particularly significant in dynamics when the characteristic length
20 λ associated with the external excitation (typical wavelength and size of
21 the domain of propagation) is not sufficiently large compared to the char-
22 acteristic internal length ℓ so as to neglect the underlying micro-structural
23 architecture. Neglected in classical theories, such characteristic inner-lengths
24 usually result in additional high-order spatial or time derivatives of relevant
25 state variables in the governing equations [8, 9, 10]. This leads to space
26 and time behavior characterized through additional material parameters to
27 estimate for numerical applications.

28 To justify such high-order derivatives, asymptotic homogenization tech-
29 niques applied to micro-lattices or heterogeneous media were presented [11,
30 12, 13, 14, 15]. Advantageously, they bring micro-macro mechanical support
31 to extended continuum models, and micro-macro relations to estimate ma-

32 terial parameters from underlying microscopic heterogeneities. For instance,
33 long-wavelength Taylor expansions of transfer functions in analogous mass-
34 spring discrete lattices have been used for that purpose [16]. Another exam-
35 ple stands in two-scale asymptotic homogenization theory for periodic media
36 [17, 18] which has proven very useful by including high-order terms in the
37 asymptotic expansions [19, 20, 21]. In particular, microstructural size effects
38 on wave dispersion, polarisation, attenuation, and mode conversions in three-
39 dimensional space were evidenced theoretically by means of two-scale asymp-
40 totic homogenization [20]. However, some continuum models developed by
41 asymptotic approaches are unstable [22, 23], due to features developing at
42 frequencies outside the initial range of the asymptotic expansions. This is
43 a critical issue, especially for time-domain calculations involving broadband
44 signals.

45 While many micro-continuum theories have been formulated by equipping
46 material particles with enriched kinematics, including rotational degrees of
47 freedom [2] or micro-deformations [3, 4, 5], another class of extended con-
48 tinuum model, called *stress gradient elasticity*, was formulated on the idea
49 that stress rather than kinematics constitutes the driving variable in the ma-
50 terial behavior. Tracing back to Eringen’s constitutive relations [24] in the
51 form of partial differential equations involving both the stress tensor and its
52 Laplacian, stress gradient elasticity found further theoretical developments
53 recently [25, 26, 27, 28] including its formulation in elastodynamics by For-
54 est & Sab [29]. These authors obtained a generalized wave equation for the
55 displacement variable U in one-dimensional (1-D) stress gradient elasticity
56 media, which involved, in addition to the classical wave-operator, its fourth-

57 order time derivative $\partial_t^4 U$ and mixed space-time derivative $\partial_t^2 \partial_x^2 U$. However,
58 the dispersion of waves in such stress gradient elasticity material was not
59 studied any further.

60 In the present work, our objective is fourfold: (i) to extend the elas-
61 todynamics stress gradient model developed by Forest & Sab [29] in one-
62 dimensional space to include space derivative $\partial_x^4 U$ in the generalized wave
63 equation; (ii) to evidence the dispersive features of wave propagation in such
64 medium; (iii) to identify all five material parameters involved in the extended
65 stress gradient model applied to heterogeneous elastic materials ; and (iv)
66 to compute the transient response of stress gradient media to transient bulk
67 sources, to be compared with direct simulations in heterogeneous Cauchy
68 media. In what follows, the *original stress gradient model* refers to the elas-
69 todynamics stress gradient model developed by Forest & Sab [29].

70 The outline of this paper is the following. In Sec. 2, we propose an
71 extended stress gradient model, which is obtained by considering an aux-
72 iliary elasticity. It is shown to be energetically consistent and stable and
73 its governing equation includes a fourth-order space derivative that did not
74 exist in the original stress gradient model. In Sec. 3, the wave dispersion,
75 phase velocity and group velocity corresponding to this model are derived
76 and discussed, in particular with respect to those of the original stress gra-
77 dient model. In Sec. 4, a relation is drawn between the proposed model
78 and higher-order homogenized models obtained from microstructured elas-
79 tic materials. This relation yields a way to identify the parameters of the
80 proposed stress gradient model for a given elastic micro-structured material,
81 while ensuring stability and energy consistency. Finally, in Sec. 5, numerical

82 simulations are proposed to illustrate the behavior of the proposed model in
 83 time, in particular with respect to stability and in comparison with other
 84 similar models proposed in the literature.

85 2. Stress gradient model

86 Properties of stress-gradient materials are analysed theoretically: hyper-
 87 bolicity, stability, existence and regularity of solutions. For the sake of gen-
 88 erality, an extended stress gradient elasticity model with three inner length
 89 scales is considered. It generalizes the recent developments on stress gradient
 90 elastodynamics with two inner lengths [29].

91 2.1. Constitutive laws

92 Let U be the particle displacement and ζ an auxiliary displacement which
 93 encapsulates the size effects. It follows the velocity v , strain e , auxiliary
 94 velocity φ and auxiliary strain θ

$$95 \quad v = \partial_t U, \quad e = \partial_x U, \quad \varphi = \partial_t \zeta, \quad \theta = \partial_x \zeta. \quad (1)$$

96 One defines the kinetic and potential energy densities \mathcal{K} and \mathcal{W}

$$97 \quad \mathcal{K} = \varrho \frac{v^2}{2} + \mu \frac{\varphi^2}{2}, \quad \mathcal{W} = \frac{E}{2}(e + \theta)^2 + \kappa \frac{\theta^2}{2} + D \frac{\zeta^2}{2}, \quad (2)$$

where ϱ is a density, μ is an auxiliary density, E is an elasticity modulus, κ
 is an auxiliary elasticity modulus and D is a stress gradient modulus. The

energy densities (2) amount to the positive quadratic forms

$$\mathcal{K} = \frac{1}{2} \begin{pmatrix} v \\ \varphi \end{pmatrix}^T \cdot \mathbb{M} \cdot \begin{pmatrix} v \\ \varphi \end{pmatrix}, \quad (3a)$$

$$\mathcal{W} = \frac{1}{2} \begin{pmatrix} e \\ \theta \end{pmatrix}^T \cdot \mathbb{E} \cdot \begin{pmatrix} e \\ \theta \end{pmatrix} + \frac{1}{2} \begin{pmatrix} U \\ \zeta \end{pmatrix}^T \cdot \mathbb{D} \cdot \begin{pmatrix} U \\ \zeta \end{pmatrix}, \quad (3b)$$

98 where \mathbb{M} , \mathbb{E} and \mathbb{D} are symmetric and positive matrices

$$99 \quad \mathbb{M} = \begin{bmatrix} \varrho & 0 \\ 0 & \mu \end{bmatrix}, \quad \mathbb{E} = \begin{bmatrix} E & E \\ E & E + \kappa \end{bmatrix}, \quad \mathbb{D} = \begin{bmatrix} 0 & 0 \\ 0 & D \end{bmatrix}. \quad (4)$$

100 Introducing the stress fields σ and τ and stress gradient R

$$101 \quad \sigma = \frac{\partial \mathcal{W}}{\partial e}, \quad \tau = \frac{\partial \mathcal{W}}{\partial \theta}, \quad R = \frac{\partial \mathcal{W}}{\partial \zeta}, \quad (5)$$

the potential energy (2) provides the constitutive laws

$$\sigma = E \partial_x (U + \zeta), \quad (6a)$$

$$\tau = E \partial_x (U + \zeta) + \kappa \partial_x \zeta, \quad (6b)$$

$$R = D \zeta. \quad (6c)$$

102 The constitutive laws of original stress gradient model are recovered when

103 $\kappa = 0$ [29].

104 2.2. Dynamic equations

Hamilton's stationary principle applied to the Lagrangian density $\mathcal{L} = \mathcal{K} - \mathcal{W}$ gives the Euler-Lagrange equations

$$\frac{\partial}{\partial t} \left(\frac{\partial \mathcal{L}}{\partial v} \right) + \frac{\partial}{\partial x} \left(\frac{\partial \mathcal{L}}{\partial e} \right) - \frac{\partial \mathcal{L}}{\partial U} = 0, \quad (7a)$$

$$\frac{\partial}{\partial t} \left(\frac{\partial \mathcal{L}}{\partial \varphi} \right) + \frac{\partial}{\partial x} \left(\frac{\partial \mathcal{L}}{\partial \theta} \right) - \frac{\partial \mathcal{L}}{\partial \zeta} = 0. \quad (7b)$$

Introducing the external bulk forces F_U and F_ζ , the dynamic equations follow from (2) and (7) in the form

$$\varrho \partial_t^2 U = \partial_x \sigma + \varrho F_U, \quad (8a)$$

$$\mu \partial_t^2 \zeta = \partial_x \tau - R + \mu F_\zeta, \quad (8b)$$

105 Multiplication of (8a) and (8b) by v and φ and summation yield the conser-
 106 vation law for energy

$$107 \quad \partial_t(\mathcal{K} + \mathcal{W}) + \partial_x(\Pi) = \mathcal{P}, \quad (9)$$

108 where the power density of external bulk forces \mathcal{P} , and the Poynting 'vector'
 109 Π are given by

$$110 \quad \mathcal{P} = \varrho F_U v + \mu F_\zeta \varphi \quad \text{and} \quad \Pi = -(\sigma v + \tau \varphi). \quad (10)$$

111 Equation (9) shows that the time variation of the energy $\mathcal{K} + \mathcal{W}$ corresponds
 112 to the power density of external bulk forces and energy fluxes described by
 113 the Poynting 'vector'.

114 2.3. Hyperbolic system

115 Equations (6) and (8) can be rewritten in the matrix form

$$116 \quad \partial_t \mathbf{W} + \mathbb{A} \cdot \partial_x \mathbf{W} = \mathbb{S} \cdot \mathbf{W} + \mathbf{F}, \quad (11)$$

with the state vector \mathbf{W} , the source \mathbf{F} and the matrices \mathbb{A} and \mathbb{S}

$$\mathbf{W} = \begin{Bmatrix} v \\ \varphi \\ \sigma \\ \tau \\ R \end{Bmatrix}, \quad \mathbb{A} = - \begin{bmatrix} 0 & 0 & 1/\varrho & 0 & 0 \\ 0 & 0 & 0 & 1/\mu & 0 \\ E & E & 0 & 0 & 0 \\ E & E + \kappa & 0 & 0 & 0 \\ 0 & 0 & 0 & 0 & 0 \end{bmatrix}, \quad (12a)$$

$$\mathbf{F} = \begin{Bmatrix} F_U \\ F_\zeta \\ 0 \\ 0 \\ 0 \end{Bmatrix}, \quad \mathbb{S} = \begin{bmatrix} 0 & 0 & 0 & 0 & 0 \\ 0 & 0 & 0 & 0 & -1/\mu \\ 0 & 0 & 0 & 0 & 0 \\ 0 & 0 & 0 & 0 & 0 \\ 0 & D & 0 & 0 & 0 \end{bmatrix}. \quad (12b)$$

The eigenvalues of \mathbb{A} and \mathbb{S} are

$$\text{Sp}(\mathbb{A}) = \{0; \pm c_{\mathbb{A}}^+; \pm c_{\mathbb{A}}^-\}, \quad (13a)$$

$$\text{Sp}(\mathbb{S}) = \{0; 0; 0; \pm i\omega_{\mathbb{S}}\}, \quad (13b)$$

117 where the characteristic speeds $c_{\mathbb{A}}^\pm$ and frequency $\omega_{\mathbb{S}}$ read

$$118 \quad c_{\mathbb{A}}^\pm = c_0 \sqrt{\frac{b_m^2 \pm \sqrt{b_m^4 - 4b_t^2 b_x^2}}{2b_t^2}} \quad \text{and} \quad \omega_{\mathbb{S}} = \sqrt{\frac{D}{\mu}}. \quad (14)$$

119 In (14), $c_0 = \sqrt{E/\varrho}$ is the classical wave speed in the Cauchy medium, and
120 the inner lengths are

$$121 \quad b_t = \sqrt{\frac{\mu}{\varrho}} B, \quad b_x = \sqrt{\frac{\kappa}{E}} B, \quad b_m = \sqrt{b^2 + b_t^2 + b_x^2}, \quad (15)$$

122 with the characteristic area $B \equiv b^2 = E/D$. The inequalities

$$123 \quad b_m^4 \geq b_m^4 - 4b_t^2 b_x^2 = (b_m^2 - 2b_t^2)^2 + 4b_t^2 \geq (b_m^2 - 2b_t^2)^2 \geq 0 \quad (16)$$

124 imply that the characteristic speeds $c_{\mathbb{A}}^{\pm}$ are real and satisfy

$$125 \quad 0 \leq c_{\mathbb{A}}^{-} \leq c_0 \leq c_{\mathbb{A}}^{+}. \quad (17)$$

126 When $\kappa \neq 0$, each eigenvalue of \mathbb{A} is associated with one single eigenvector

$$127 \quad \mathbf{W}_{\mathbb{A}}(c \neq 0) = \begin{Bmatrix} 1 \\ \left(\frac{c^2}{c_0^2} - 1\right) \\ \varrho c \\ \left(\frac{c^2}{c_0^2} - 1\right) \mu c \\ 0 \end{Bmatrix}, \quad \mathbf{W}_{\mathbb{A}}(0) = \begin{Bmatrix} 0 \\ 0 \\ 0 \\ 0 \\ 1 \end{Bmatrix}. \quad (18)$$

128 The matrix \mathbb{A} is thus diagonalizable with real eigenvalues, which proves the
 129 hyperbolicity of (11) [30]. Also, the eigenvalues of \mathbb{S} are either null or purely
 130 imaginary, which implies that $\mathbf{W} \equiv \mathbf{0}$ is asymptotically stable [30]. Intro-
 131 ducing the definite positive symmetric matrix

$$132 \quad \mathbb{Q} = \begin{bmatrix} \varrho & 0 & 0 & 0 & 0 \\ 0 & \mu & 0 & 0 & 0 \\ 0 & 0 & 1/E + 1/\kappa & -1/\kappa & 0 \\ 0 & 0 & -1/\kappa & 1/\kappa & 0 \\ 0 & 0 & 0 & 0 & 1/D \end{bmatrix} \quad (19)$$

133 the following relations hold

$$134 \quad \mathbb{Q}\mathbb{A} = - \begin{bmatrix} 0 & 0 & 1 & 0 & 0 \\ 0 & 0 & 0 & 1 & 0 \\ 1 & 0 & 0 & 0 & 0 \\ 0 & 1 & 0 & 0 & 0 \\ 0 & 0 & 0 & 0 & 0 \end{bmatrix}, \quad \mathbb{Q}\mathbb{S} = \begin{bmatrix} 0 & 0 & 0 & 0 & 0 \\ 0 & 0 & 0 & 0 & -1 \\ 0 & 0 & 0 & 0 & 0 \\ 0 & 0 & 0 & 0 & 0 \\ 0 & 1 & 0 & 0 & 0 \end{bmatrix}. \quad (20)$$

These relations imply that matrix \mathbb{Q} is a symmetrizer for the system (11), in the sense that $\mathbb{Q}\mathbb{A}$ is symmetric, and $\mathbb{Q}\mathbb{S}$ is skew-symmetric with null diagonal terms [32]. One has

$$\mathbf{W}^T \mathbb{Q} \partial_t \mathbf{W} = \partial_t (\mathcal{K} + \mathcal{W}), \quad \mathbf{W}^T \mathbb{Q} \mathbf{F} = \mathcal{P}, \quad (21a)$$

$$\mathbf{W}^T (\mathbb{Q}\mathbb{A}) \partial_x \mathbf{W} = \partial_x (\Pi), \quad \mathbf{W}^T (\mathbb{Q}\mathbb{S}) \mathbf{W} = 0, \quad (21b)$$

135 As a result, multiplication of (11) by $\mathbf{W}^T \mathbb{Q}$ while using (21) recovers the
 136 equation of energy conservation (9). Moreover, the symmetrizer allows to use
 137 Friedrichs' theory on symmetric systems [31]: assuming sufficiently smooth
 138 initial data and excitation, it yields existence and regularity of the solution
 139 to (12). Details are given in section 3-2 and Theorem 3-1 of [40].

140 In the case of the original stress gradient model $\kappa = 0$, then $\tau = \sigma$. It
 141 reduces the system in Eq. (12) to

$$142 \quad \partial_t \mathbf{W}^* + \mathbb{A}^* \cdot \partial_x \mathbf{W}^* = \mathbb{S}^* \cdot \mathbf{W}^* + \mathbf{F}^*, \quad (22)$$

where the reduced vectors and matrices are

$$\mathbf{W}^* = \begin{Bmatrix} v \\ \varphi \\ \sigma \\ R \end{Bmatrix}, \quad \mathbb{A}^* = - \begin{bmatrix} 0 & 0 & 1/\varrho & 0 \\ 0 & 0 & 1/\mu & 0 \\ E & E & 0 & 0 \\ 0 & 0 & 0 & 0 \end{bmatrix}, \quad (23a)$$

$$\mathbf{F}^* = \begin{Bmatrix} F_U \\ F_\zeta \\ 0 \\ 0 \end{Bmatrix}, \quad \mathbb{S}^* = \begin{bmatrix} 0 & 0 & 0 & 0 \\ 0 & 0 & 0 & -1/\mu \\ 0 & 0 & 0 & 0 \\ 0 & D & 0 & 0 \end{bmatrix}. \quad (23b)$$

The eigenvalues of reduced matrices \mathbb{A}^* and \mathbb{S}^* are

$$\text{Sp}(\mathbb{A}^*) = \{0; 0; \pm c_{\mathbb{A}}^*\}, \quad (24a)$$

$$\text{Sp}(\mathbb{S}^*) = \{0; 0; \pm i\omega_{\mathbb{S}}\}, \quad (24b)$$

143 Here, the second zero in the spectrum of \mathbb{A}^* is inherited from the eigenvalue
 144 $\pm c_{\mathbb{A}}^-$ of \mathbb{A} which is zero when $\kappa = 0$ (14). The eigenvalue $c_{\mathbb{A}}^*$ is equal to $c_{\mathbb{A}}^+$
 145 calculated with the modulus $\kappa = 0$,

$$146 \quad c_{\mathbb{A}}^* = c_0 \sqrt{\frac{\varrho + \mu}{\mu}} \geq c_0. \quad (25)$$

147 The eigenvectors associated with the eigenvalues of \mathbb{A}^* read

$$148 \quad \mathbf{W}_{\mathbb{A}}^*(\pm c_{\mathbb{A}}^*) = \begin{Bmatrix} 1 \\ \varrho/\mu \\ \pm \varrho c_{\mathbb{A}}^* \\ 0 \end{Bmatrix}, \quad \mathbf{W}_{\mathbb{A}}^*(0) = \text{Vect} \left(\begin{Bmatrix} 0 \\ 0 \\ 0 \\ 1 \end{Bmatrix}, \begin{Bmatrix} 1 \\ -1 \\ 0 \\ 0 \end{Bmatrix} \right). \quad (26)$$

149 The reduced matrix \mathbb{A}^* is thus diagonalizable with real eigenvalues. A sym-
 150 metrizer for the system (22) is

$$151 \quad \mathbb{Q}^* = \text{diag}(\varrho; \mu; 1/E; 1/D). \quad (27)$$

152 As a consequence, all the properties of the full system are still valid in the
 153 case of the reduced system (22).

154 2.4. High-order wave equations

Now, combination of Eqs. (6a) to (8a) yields

$$\varrho \partial_t^2 U - E \partial_x^2 U + \mathcal{H}(U) = \varrho F_U + \Psi_U, \quad (28a)$$

$$\varrho \partial_t^2 \zeta - E \partial_x^2 \zeta + \mathcal{H}(\zeta) = \Psi_{\zeta}. \quad (28b)$$

Here, the classical wave operator $\varrho \partial_t^2 \bullet - E \partial_x^2 \bullet$ is accompanied by higher order derivatives, described by the operator $\mathcal{H}(\bullet)$ and forcing terms Ψ_U and Ψ_ζ

$$\mathcal{H}(\bullet) = \frac{\varrho^2 b_t^2}{E} \partial_t^4(\bullet) + E b_x^2 \partial_x^4(\bullet) - \varrho b_m^2 \partial_t^2 \partial_x^2(\bullet), \quad (29a)$$

$$\Psi_U = \frac{\varrho^2 b_t^2}{E} \partial_t^2 F_U - \varrho \partial_x^2 [(b_m^2 - b_t^2) F_U - b_t^2 F_\zeta], \quad (29b)$$

$$\Psi_\zeta = \frac{\varrho^2 b_t^2}{E} \partial_t^2 F_\zeta - \varrho \partial_x^2 [b_t^2 F_\zeta - b^2 F_U], \quad (29c)$$

155 where the lengths b_t , b_x and b_m are given in (15). Derivatives ∂_x^4 , $\partial_x^2 \partial_t^2$ and
 156 ∂_t^4 of the displacements are present in (28), while only terms in $\partial_x^2 \partial_t^2$ and ∂_t^4
 157 are present in the original stress gradient model. The latter is shown to be
 158 causal in the next section: the postulated causality condition introduced by
 159 Metrikine [33], which states that leading-order derivatives in space and time
 160 should be of the same order, is therefore clearly not necessary.

161 Displacement U and auxiliary displacement ζ are not forced by the same
 162 source in (28a) and (28b). In the absence of source, they satisfy the same
 163 high-order wave equation in the form $\varrho \partial_t^2 \bullet - E \partial_x^2 \bullet + \mathcal{H}(\bullet) = 0$.

164 3. Wave dispersion in stress gradient media

165 In this section, wave dispersion with inner lengths is studied. Existence
 166 of supplementary modes when $\kappa \neq 0$ is examined. Lastly, causality is proven,
 167 whatever κ .

168 3.1. Dispersion relation

169 Plane wave of the form $U = e^{i(kx - \omega t)}$ is considered, where ω is the angular
 170 frequency and k is the wavenumber. Substitution into the high-order wave

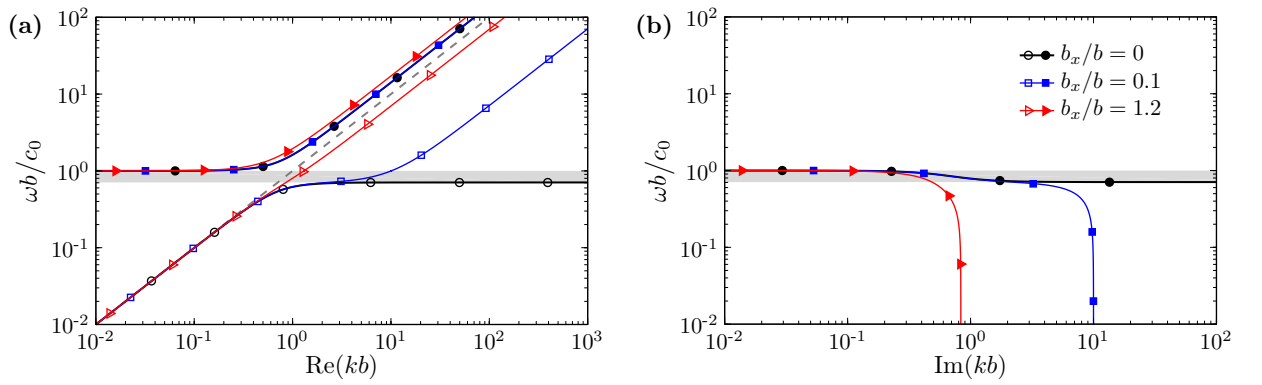


Figure 1: (Color online) Dispersion relation in stress gradient media. Modes with (a) real positive and (b) imaginary positive normalised wavenumbers kb versus normalised frequency $\omega b/c_0$. Here, filled or empty symbols stand for different modes. Hence, modes with real (propagative) and imaginary (exponentially-decaying) wavenumbers are distinct, and do not correspond to real and imaginary parts of a same wavenumber. Calculations with normalised inner lengths $b_t/b = 1$ and various b_x/b . Grey zone is bandgap when $b_x = 0$. Dashed grey line corresponds to elastodynamic relation $kb = \omega b/c_0$. Legend in (a) is the same as in (b).

171 equation leads to

$$172 \quad - \left(1 - \frac{\varrho\omega^2}{E}b_t^2\right) \frac{\varrho\omega^2}{E} + \left(1 - \frac{\varrho\omega^2}{E}b_m^2\right) k^2 + b_x^2 k^4 = 0. \quad (30)$$

173 In the limit case $B = 0$, inner-lengths vanish $b_x = b_m = b_t = 0$, and one
174 recovers the Cauchy dispersion relation

$$175 \quad k = \pm k_0 \quad \text{with} \quad k_0 = \omega \sqrt{\frac{\varrho}{E}} = \frac{\omega}{c_0}. \quad (31)$$

176 Now, wave dispersion in stress gradient media with inner-lengths is studied.
177 To illustrate the discussion, normalised dispersion curves and wave velocities
178 are presented in Figs. 1 and 2. The angular frequencies ω_t and ω_m , such that
179 $k_0 b_t = 1$ and $k_0 b_m = 1$, are introduced. They write

$$180 \quad \omega_t = \omega_{\mathbb{S}} = \sqrt{\frac{D}{\mu}}, \quad \omega_m = \sqrt{\frac{D}{\varrho \left(1 + \frac{\kappa}{E}\right) + \mu}} \leq \omega_t, \quad (32)$$

where $i\omega_{\mathbb{S}}$ is an eigenvalue of \mathbb{S} (11). The biquadratic dispersion equation
(30) admits four roots

$$k_{\pm}^{\text{I}} = \pm k_0 \sqrt{\frac{2(1 - (k_0 b_t)^2)}{1 - (k_0 b_m)^2 + \sqrt{\Delta}}}, \quad (33a)$$

$$k_{\pm}^{\text{II}} = \pm k_0 \sqrt{\frac{2(1 - (k_0 b_t)^2)}{1 - (k_0 b_m)^2 - \sqrt{\Delta}}}. \quad (33b)$$

181 From (15), the discriminant Δ satisfies

$$182 \quad \begin{aligned} \Delta &= (1 - (k_0 b_m)^2)^2 + 4(k_0 b_x)^2 (1 - (k_0 b_t)^2), \\ &= (1 - (k_0 b_m)^2 + 2(k_0 b_x)^2)^2 + 4(k_0 b)^2 (k_0 b_x)^2 \geq 0. \end{aligned} \quad (34)$$

183 In the low frequency range $k_0 b_x \ll 1$, $k_0 b_t \ll 1$ and $k_0 b_m \ll 1$, a Taylor
184 expansion of (33) provides the approximates

$$185 \quad k_{\pm}^{\text{I}} \sim \pm k_0 \left(1 + \frac{1}{2} k_0^2 B\right) \quad \text{and} \quad k_{\pm}^{\text{II}} \sim \pm \frac{i}{b_x}. \quad (35)$$

186 The first two branches with purely real wavenumbers k_{\pm}^{I} are propagative.
 187 Their Taylor expansion is asymptotic to $\pm k_0 = \pm\omega/c_0$, and deviation from
 188 this line is driven by the stress gradient parameter B . The two other branches
 189 with purely-imaginary wavenumbers k_{\pm}^{II} in (35) correspond to non-oscillating
 190 exponentially-decaying displacements.

191 At high frequencies $k_0 b_x \gg 1$, $k_0 b_t \gg 1$ and $k_0 b_m \gg 1$, the wavenumbers
 192 satisfy

$$193 \quad k_{\pm}^{\text{I}} \sim \pm \frac{\omega}{c_{\mathbb{A}}^-} \quad \text{and} \quad k_{\pm}^{\text{II}} \sim \pm \frac{\omega}{c_{\mathbb{A}}^+}, \quad (36)$$

194 where wave speeds $c_{\mathbb{A}}^{\pm} \geq 0$ are eigenvalues of \mathbb{A} (14). One recalls $c_{\mathbb{A}}^- \leq c_0$ and
 195 $c_{\mathbb{A}}^+ \geq c_0$ in (17).

196 At the intermediate frequency $\omega_t = \omega_{\mathbb{S}}$ such that $k_0 b_t = 1$, the discrimi-
 197 nant (34) yields $\sqrt{\Delta} = |1 - (k_0 b_m)^2|$, which provides $k_{\pm}^{\text{II}} = \pm 0$. This property
 198 holds for both the original stress gradient model ($b_x = 0$) and the extended
 199 one ($b_x \neq 0$).

Finally, as inner length b_x reaches zero in (33), the dispersion relation for
 the original stress gradient model is recovered

$$k_{\pm}^{\text{I}} = \pm k_0 \sqrt{\frac{1 - (k_0 b_t)^2}{1 - (k_0 b_m)^2}}, \quad k_{\pm}^{\text{II}} = \pm \infty, \quad \text{if } \omega < \omega_m, \quad (37a)$$

$$k_{\pm}^{\text{I}} = \pm \infty, \quad k_{\pm}^{\text{II}} = \pm k_0 \sqrt{\frac{1 - (k_0 b_t)^2}{1 - (k_0 b_m)^2}}, \quad \text{if } \omega > \omega_m. \quad (37b)$$

200 While four modes are supported in stress gradient media in the extended
 201 model ($b_x \neq 0$), only two of them exist in the original model ($b_x = 0$);
 202 the wavenumbers of the two others are sent to infinity. Finally, in the fre-
 203 quency range $[\omega_m, \omega_t]$, the wavenumber in the original stress gradient mate-
 204 rial becomes purely imaginary, see (37b), which leads to non-oscillating and

205 exponentially-decaying displacements with $\text{Im}(k_{\pm}^{\text{II}}) > 0$.

206 3.2. Phase velocity and group velocity

207 Phase velocity c_{p} and group velocity c_{g} are defined by

$$208 \quad c_{\text{p}}(k_{\text{R}}) = \frac{\bar{\omega}(k_{\text{R}})}{k_{\text{R}}} \quad \text{and} \quad c_{\text{g}}(k_{\text{R}}) = \frac{\text{d}\bar{\omega}(k_{\text{R}})}{\text{d}k_{\text{R}}}, \quad (38)$$

209 where the angular frequency $\bar{\omega}(k_{\text{R}})$ is solution to the dispersion equation
 210 (30) with the real-valued wavenumber $k = k_{\text{R}}$ being prescribed. Whether
 211 in the original ($b_x = 0$) or the extended ($b_x \neq 0$) stress gradient model, the
 212 ω -biquadratic dispersion equation (30) admits the four solutions

$$213 \quad \bar{\omega}_{\pm}^{\text{I}}(k_{\text{R}}) = \pm k_{\text{R}} c_{\text{p}}^{\text{I}}(k_{\text{R}}) \quad \text{and} \quad \bar{\omega}_{\pm}^{\text{II}}(k_{\text{R}}) = \pm k_{\text{R}} c_{\text{p}}^{\text{II}}(k_{\text{R}}), \quad (39)$$

where the phase velocities $c_{\text{p}}^{\text{I}}(k_{\text{R}})$ and $c_{\text{p}}^{\text{II}}(k_{\text{R}})$ are given by

$$214 \quad \frac{c_{\text{p}}^{\text{I}}(k_{\text{R}})}{c_0} = \sqrt{\frac{1 + (k_{\text{R}}b_m)^2 - \sqrt{\Delta_c}}{2(k_{\text{R}}b_t)^2}}, \quad (40a)$$

$$215 \quad \frac{c_{\text{p}}^{\text{II}}(k_{\text{R}})}{c_0} = \sqrt{\frac{1 + (k_{\text{R}}b_m)^2 + \sqrt{\Delta_c}}{2(k_{\text{R}}b_t)^2}}. \quad (40b)$$

214 Here the discriminant Δ_c reads

$$215 \quad \begin{aligned} \Delta_c &= (1 + (k_{\text{R}}b_m^2)^2)^2 - 4(k_{\text{R}}b_t)^2(1 + (k_{\text{R}}b_x)^2), \\ &= (1 + k_{\text{R}}^2(B + b_x^2 - b_t^2))^2 + 4k_{\text{R}}^4Bb_t^2. \end{aligned} \quad (41)$$

216 Since $B \geq 0$, the following inequalities result from (41)

$$217 \quad \Delta_c \geq (1 + k_{\text{R}}^2(b_m^2 - 2b_t^2))^2 > 0, \quad \sqrt{\Delta_c} \leq 1 + (k_{\text{R}}b_m)^2. \quad (42)$$

218 It implies that phase velocities $c_{\text{p}}^{\text{I}}(k_{\text{R}})$ and $c_{\text{p}}^{\text{II}}(k_{\text{R}})$ are real-valued and positive,
 219 and satisfy

$$220 \quad 0 < c_{\text{p}}^{\text{I}}(k_{\text{R}}) \leq c_0 \leq c_{\text{p}}^{\text{II}}(k_{\text{R}}). \quad (43)$$

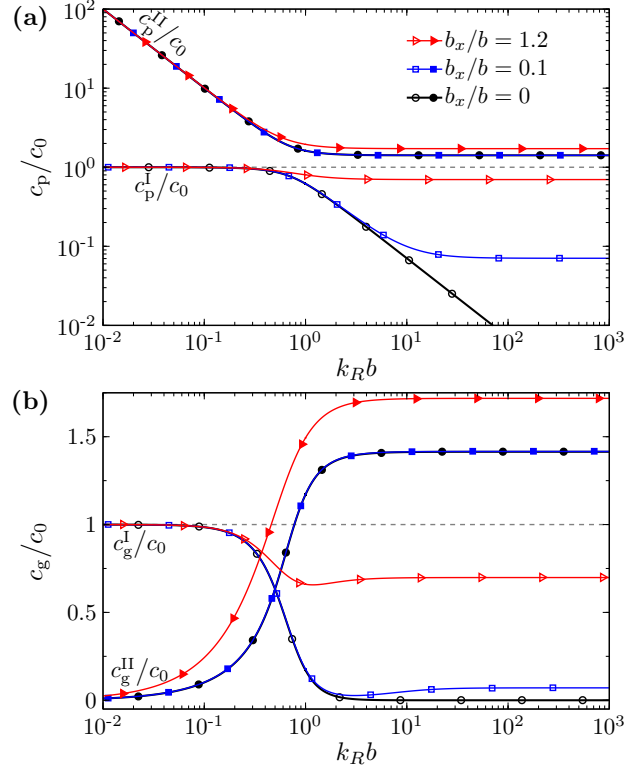


Figure 2: (Color online) Dispersion relation in stress gradient media: (a) normalised phase velocities c_p/c_0 and (b) normalised group velocities c_g/c_0 versus normalised wavenumber $k_R b$ for modes I and II. Here, filled or empty symbols stand for different modes. Symbols consistent with Fig. 1. Calculations with normalised inner lengths $b_t/b = 1$ and various b_x/b . Dashed grey line corresponds to $c_p = c_g = c_0$. Legend in (b) is the same as in (a).

Moreover, the phase velocities are smooth even functions of the wavenumber k_R , and display the limits

$$c_p^I(k_R) \rightarrow c_0, \quad c_p^{II}(k_R) \sim \frac{c_0}{|k_R b_t|}, \quad \text{as } |k_R| \rightarrow 0, \quad (44a)$$

$$c_p^I(k_R) \rightarrow c_A^-, \quad c_p^{II}(k_R) \rightarrow c_A^+, \quad \text{as } |k_R| \rightarrow \infty. \quad (44b)$$

221 Derivation of (39) with respect to k_R provides

$$222 \quad \frac{d\bar{\omega}_{\pm}^I(k_R)}{dk_R} = \pm c_g^I(k_R) \quad \text{and} \quad \frac{d\bar{\omega}_{\pm}^{II}(k_R)}{dk_R} = \pm c_g^{II}(k_R) \quad (45)$$

where, accounting for Eq. (40),

$$c_g^I(k_R) = \left\{ 1 - \frac{1}{\sqrt{\Delta_c}} \left(\left(\frac{c_0}{c^I(k_R)} \right)^2 - 1 \right) \right\} c_p^I(k_R), \quad (46a)$$

$$c_g^{II}(k_R) = \left\{ 1 - \frac{1}{\sqrt{\Delta_c}} \left(1 - \left(\frac{c_0}{c^{II}(k_R)} \right)^2 \right) \right\} c_p^{II}(k_R). \quad (46b)$$

223 As a result of (43), one has

$$224 \quad c_g^I(k_R) \leq c_p^I(k_R) \leq c_0, \quad \text{and} \quad c_g^{II}(k_R) \leq c_p^{II}(k_R). \quad (47)$$

Equation (46) shows that group velocities are smooth and even functions of k_R , and display the limits

$$c_g^I(k_R) = c_0, \quad c_g^{II}(k_R) = 0, \quad \text{as } |k_R| = 0, \quad (48a)$$

$$c_g^I(k_R) \rightarrow c_A^-, \quad c_g^{II}(k_R) \rightarrow c_A^+, \quad \text{as } |k_R| \rightarrow \infty, \quad (48b)$$

225 As a consequence, the group velocities are bounded whatever b_x , which
 226 complies with causality. The postulated causality condition introduced by
 227 Metrikine [33], which is not satisfied when $b_x = 0$, is therefore clearly not
 228 necessary.

229 4. Micro-macro calculation of material parameters

230 It was shown in Sec. 2.2 that the displacement U in the stress gradient
 231 model satisfies the following equation, according to Eqs. (28) and (29),

$$232 \quad \begin{aligned} & \varrho \partial_t^2 U - E \partial_x^2 U + \frac{\varrho^2}{E} b_t^2 \partial_t^4 U + E b_x^2 \partial_x^4 U - \varrho b_m^2 \partial_t^2 \partial_x^2 U, \\ & = \varrho F_U + \frac{\varrho^2 b_t^2}{E} \partial_t^2 F_U - \varrho \partial_x^2 [(b_m^2 - b_t^2) F_U - b_t^2 F_C]. \end{aligned} \quad (49)$$

233 Here we show that (49) stands for an effective description of micro-structured
 234 media in the low-frequency range. To this end, a micro-macro homogeniza-
 235 tion scheme is presented, which provides (i) the micro-mechanical background
 236 to (49); and (ii) a method to estimate the material parameters in the stress
 237 gradient model. It relies on the theory of two-scale asymptotic homoge-
 238 nization [17, 18] wherein high-order terms of the asymptotic expansions are
 239 included [19, 20, 21].

240 4.1. High-order asymptotic homogenization

The homogenization model starts from the equations of dynamic equi-
 librium and elasticity at the microstructural scale of the one-dimensional
 medium

$$\rho \partial_t^2 u = \partial_x s + \rho f, \quad (50a)$$

$$s = a \partial_x u, \quad (50b)$$

241 where u and s are the micro-structural displacement and stress fields, ρ and
 242 a the density and elastic modulus, and f is the bulk force in the micro-
 243 structure. The heterogeneous medium consists of the 1-D periodic repetition
 244 of a Representative Elementary Volume (REV) Ω of length ℓ .

245 A scale separation is assumed, whereby the characteristic macroscopic
 246 length λ (related to the reduced wavelength $\mathcal{O}(1/k_0)$ or size of the domain of
 247 propagation) is much larger than ℓ . This condition is quantified by the scale
 248 parameter $\epsilon = \ell/\lambda \ll 1$ and enables the application of two-scale asymptotic
 249 homogenization. To account for both scales, the two space variables x and
 250 $y = \epsilon^{-1}x$ are defined for macro- and microscopic description respectively.
 251 Material parameter $\rho(y)$ and $a(y)$ are set to depend on y , and are ℓ -periodic

252 over y . No high material contrast between the heterogeneities is considered:
 253 the local density $\rho(y)$ and elastic modulus $a(y)$ are assumed to vary only
 254 moderately around their mean values, $\rho(y) = \mathcal{O}(\langle \rho \rangle)$ and $a(y) = \mathcal{O}(\langle a \rangle)$,
 255 where the y -averaging operator $\langle \cdot \rangle$ is defined by

$$256 \quad \langle \cdot \rangle = \frac{1}{\ell_y} \int_{\Omega} \cdot \, dy \quad \text{with} \quad \ell_y = \int_{\Omega} 1 \, dy. \quad (51)$$

The homogenization of media with inner resonance due to high material contrasts is therefore out of the scope of the present study [34, 35]. Also, the propagative medium is supposed to be macroscopically homogeneous, which implies that $\rho(y)$ and $a(y)$ are independent of the variable x of macroscopic description. The fields $u(x, y)$ and $s(x, y)$ can display variation at both micro- and macroscopic scales, and they are set to depend on both x and y , while being ℓ -periodic over y . This implies to modify spacial differential operator ∂_x into $\partial_x + \epsilon^{-1}\partial_y$. Finally, the displacement and stress are expanded asymptotically into powers of the scale parameter ϵ according to

$$u(x, y) = u^{(0)} + \epsilon u^{(1)} + \epsilon^2 u^{(2)} + \epsilon^3 u^{(3)} + \mathcal{O}(\epsilon^4), \quad (52a)$$

$$s(x, y) = s^{(0)} + \epsilon s^{(1)} + \epsilon^2 s^{(2)} + \mathcal{O}(\epsilon^3), \quad (52b)$$

257 where bracketed superscripts indicate the order of the terms and all terms
 258 $u^{(j)}(x, y)$ and $s^{(j)}(x, y)$ for $j \geq 0$ are two-scale fields that depend on both
 259 x and y . The aim of high-order asymptotic homogenization is to determine
 260 not only the leading-order terms $u^{(0)}$ and $s^{(0)}$, but also higher-order terms
 261 $u^{(j)}(x, y)$ and $s^{(j)}(x, y)$ for $j \geq 1$. To do so, asymptotic expansions (52) are
 262 substituted into the governing equations (50) expressed with two-scale differ-
 263 ential operator $\partial_x + \epsilon^{-1}\partial_y$. Terms of equal power of ϵ are collected to provide
 264 problems which are solved in increasing order of the power of ϵ . Details of

265 the asymptotic homogenization procedure are provided in [Appendix A](#) and
 266 the main results with respect to the estimation of material parameters in the
 267 stress gradient model are discussed here.

268 The effective macroscopic description of the 1-D periodic elastic material
 269 relies on the displacements $\mathcal{U}^{(j)}(x)$ for $j \geq 0$, which correspond to the local
 270 mean-value of $u^{(j)}(x, y)$ in [\(52a\)](#)

$$271 \quad \mathcal{U}^{(j)}(x) = \langle u^{(j)}(x, y) \rangle. \quad (53)$$

They satisfy the governing equations

$$\mathcal{C}_0^{(0)}(\mathcal{U}^{(0)}) = \rho_0 \mathbf{f}(x), \quad (54a)$$

$$\mathcal{C}_0^{(0)}(\mathcal{U}^{(1)}) = -\rho_0 h^{(1)} \partial_x \mathbf{f}(x), \quad (54b)$$

$$\mathcal{C}_0^{(0)}(\mathcal{U}^{(2)}) = \rho_0 (h^{(1)})^2 \partial_x^2 \mathbf{f}(x) - \mathcal{C}_2^{(2)}(\mathcal{U}^{(0)}), \quad (54c)$$

where the operators $\mathcal{C}_0^{(0)}$ and $\mathcal{C}_2^{(2)}$ read

$$\mathcal{C}_0^{(0)}(\mathcal{U}^{(j)}) = \rho_0 \partial_t^2 \mathcal{U}^{(j)} - E_0 \partial_x^2 \mathcal{U}^{(j)} \quad (55a)$$

$$\mathcal{C}_2^{(2)}(\mathcal{U}^{(0)}) = -\rho_0 \Gamma_t^{(2)} \partial_x^2 \partial_t^2 \mathcal{U}^{(0)} - E_0 \Gamma_x^{(2)} \partial_x^4 \mathcal{U}^{(0)}. \quad (55b)$$

In [\(54\)](#) and [\(55\)](#), the density ρ_0 [kg/m³], elastic modulus E_0 [Pa], and characteristic length $h^{(1)}$ [m] and surfaces $\Gamma_t^{(2)}$ and $\Gamma_x^{(2)}$ [m²] satisfy micro-macro relations involving volume averages of Ω -periodic fields:

$$\rho_0 = \langle \rho \rangle > 0, \quad E_0 = \langle q_0^{(0)} \rangle > 0, \quad (56a)$$

$$h^{(1)} = \frac{\langle \rho \chi_1^{(1)} \rangle}{\langle \rho \rangle} = \frac{\langle q_1^{(1)} \rangle}{\langle q_0^{(0)} \rangle}, \quad (56b)$$

$$\Gamma_x^{(2)} = \frac{\langle q_2^{(2)} \rangle}{\langle q_0^{(0)} \rangle}, \quad \Gamma_t^{(2)} = J_1^{(2)} - \frac{\langle \rho \chi_2^{(2)} \rangle}{\langle \rho \rangle}, \quad (56c)$$

$$\text{with } J_1^{(2)} = \left\langle \frac{\rho}{\rho_0} (\chi_1^{(1)})^2 \right\rangle - \left\langle \frac{\rho}{\rho_0} \chi_1^{(1)} \right\rangle^2 > 0. \quad (56d)$$

The Ω -periodic fields $\chi_j^{(j)}(y)$ [m^j] and generalised stresses $q_j^{(j)}(y)$ [$\text{Pa}\cdot\text{m}^{j-1}$] satisfy recurrent cell problems for $j \geq 0$

$$q_j^{(j)}(y) = a \left(\chi_j^{(j)}(y) + \partial_y \chi_{j+1}^{(j+1)} \right), \quad (57a)$$

$$\partial_y q_j^{(j)} = \frac{\rho(y)}{\langle \rho \rangle} \langle q_{j-1}^{(j-1)} \rangle - q_{j-1}^{(j-1)}(y), \quad (57b)$$

$$\langle \chi_j^{(j)} \rangle = 0 \quad \text{for } j \geq 1, \quad (57c)$$

$$\chi_0^{(0)}(y) \equiv 1 \quad \text{and} \quad q_{-1}^{(-1)}(y) \equiv 0. \quad (57d)$$

272 These cell problems (57) correspond to the static equilibrium of the periodic
 273 material under Ω -periodic bulk excitation. Except for the effective density
 274 ρ_0 which depends only on $\rho(y)$, and the elasticity modulus E_0 , which de-
 275 pends only on $a(y)$, all the other high-order material parameters $h^{(1)}$, $\Gamma_t^{(2)}$
 276 and $\Gamma_x^{(2)}$ depend on both $\rho(y)$ and $a(y)$ through the cell problems. Hence,
 277 they cannot be distinguished as parameters related to either micro-inertia or
 278 micro-elasticity.

279 All macro-displacements $\mathcal{U}^{(j)}$ in (55) are governed by the classical wave
 280 operator encoded within $\mathcal{C}_0^{(0)}$ in (55a), but with different forcing sources on
 281 the right-hand-side. First, as the order j of $\mathcal{U}^{(j)}$ increases, high-order space
 282 derivatives $\partial_x^j f(x)$ of f are involved. Second, the leading-order term $\mathcal{U}^{(0)}$ and
 283 the corrector $\mathcal{U}^{(1)}$ are forced only by the bulk force f through its high-order
 284 space derivatives, while $\mathcal{U}^{(2)}$ is forced in addition by 4th-order space and time
 285 derivatives of the leading-order field $\mathcal{U}^{(0)}$. This is the clue to evidence the
 286 stress gradient dynamics operating in this low-frequency range. Third, the
 287 classical description of a Cauchy medium is recovered in the leading-order
 288 description $\mathcal{U}^{(0)}$, which can be sufficient when $\epsilon \lll 1$.

289 *4.2. Identification of stress gradient parameters*

290 Equations (54) are re-scaled to physical scale. To do so, (54b) and (54c)
 291 are multiplied by ϵ and ϵ^2 respectively, and results are summed altogether
 292 with (54a) to provide

$$293 \quad \mathcal{C}_0^{(0)}(\mathcal{U}) = \rho_0 \mathcal{F} - \epsilon^2 \mathcal{C}_2^{(2)}(\mathcal{U}^{(0)}) + \mathcal{O}(\epsilon^3), \quad (58)$$

where effective displacement \mathcal{U} and bulk force \mathcal{F} read

$$\mathcal{U}(x) = \mathcal{U}^{(0)} + \epsilon^1 \mathcal{U}^{(1)} + \epsilon^2 \mathcal{U}^{(2)} = \langle u \rangle + \mathcal{O}(\epsilon^3), \quad (59a)$$

$$\mathcal{F}(x) = f(x) - h \partial_x f(x) + h^2 \partial_x^2 f(x). \quad (59b)$$

294 Here, (59b) represents the micro-macro relation between bulk force $f(x)$ ex-
 295 perienceed at the micro-structural scale, and the resulting bulk force $\mathcal{F}(x)$
 296 emerging from it at the macroscopic scale. In particular, this micro-macro
 297 relation involves the characteristic inner-length $h = \epsilon h^{(1)}$ related to the bulk
 298 force.

299 The effective macroscopic displacement \mathcal{U} in (58) is forced not only by
 300 the effective bulk force \mathcal{F} but also by fourth-order time and space derivatives
 301 $\partial_x^2 \partial_t^2 \mathcal{U}^{(0)}$ and $\partial_x^4 \mathcal{U}^{(0)}$ of the leading-order displacement $\mathcal{U}^{(0)}$, see $\mathcal{C}_2^{(2)}$ in (55b).
 302 Meanwhile, $\mathcal{U}^{(0)}$ satisfies the classical wave equation (54a), which yields after
 303 ∂_t^2 - and ∂_x^2 - differentiation

$$304 \quad \partial_t^2 \partial_x^2 \mathcal{U}^{(0)} = \frac{\rho_0}{E_0} \{ \partial_t^4 \mathcal{U}^{(0)} - \partial_t^2 f \} = \frac{E_0}{\rho_0} \partial_x^4 \mathcal{U}^{(0)} + \partial_x^2 f. \quad (60)$$

305 Similar relations without bulk forces $f(x)$ were used in early studies [20] to
 306 define the cell problems, and more recently [11, 14] to define families of
 307 effective high-order continuum media. Indeed, this capacity to transform

308 *arbitrarily* any 4th-order time-space derivatives of $\mathcal{U}^{(0)}$ into any other ones
 309 results in the non-uniqueness of effective continuum models in the asymptotic
 310 framework [15]. The general relation is derived in [Appendix A](#) using (60)

$$\begin{aligned}
 \mathcal{C}_2^{(2)}(\mathcal{U}^{(0)}) &= \frac{\rho_0^2}{E_0} \alpha_t \Gamma_t^{(2)} \partial_t^4 \mathcal{U}^{(0)} + E_0 \alpha_x \Gamma_x^{(2)} \partial_x^4 \mathcal{U}^{(0)} \\
 311 \quad &- \rho_0 \left[(1 + \alpha_x) \Gamma_x^{(2)} + (1 + \alpha_t) \Gamma_t^{(2)} \right] \partial_x^2 \partial_t^2 \mathcal{U}^{(0)} \quad (61) \\
 &+ \rho_0 (1 + \alpha_x) \Gamma_x^{(2)} \partial_x^2 \mathcal{f} - \frac{\rho_0^2}{E_0} \alpha_t \Gamma_t^{(2)} \partial_t^2 \mathcal{f},
 \end{aligned}$$

312 where α_t and α_x are arbitrary dimensionless numbers. However, constraints
 313 are imposed further to ensure hyperbolicity and stability of the resulting
 314 model. Such aspects have been overlooked in previous studies, see [11] and
 315 references therein.

316 To conclude, (61) is substituted into (58). The latter actually holds up
 317 to $\mathcal{O}(\epsilon^3)$, hence terms of order $\mathcal{O}(\epsilon^3)$ can be added to result in equivalent
 318 models. This property is used to identify $\epsilon^2 \mathcal{U}^{(0)}$ with $\epsilon^2 \mathcal{U}$ and $\epsilon^2 \mathcal{f}(x)$ with
 319 $\epsilon^2 \mathcal{F}$ in the expression of $\epsilon^2 \mathcal{C}_2^{(2)}(\mathcal{U}^{(0)})$. Then, characteristic surface areas are
 320 re-scaled according to $\Gamma_x = \epsilon^2 \Gamma_x^{(2)}$ and $\Gamma_t = \epsilon^2 \Gamma_t^{(2)}$, which finally leads to the
 321 following high-order wave equation

$$\begin{aligned}
 \rho_0 \partial_t^2 \mathcal{U} - E_0 \partial_x^2 \mathcal{U} + \frac{\rho_0^2}{E_0} \alpha_t \Gamma_t \partial_t^4 \mathcal{U} + E_0 \alpha_x \Gamma_x \partial_x^4 \mathcal{U} \\
 322 \quad &- \rho_0 [(1 + \alpha_x) \Gamma_x + (1 + \alpha_t) \Gamma_t] \partial_x^2 \partial_t^2 \mathcal{U} \quad (62) \\
 &= \rho_0 \mathcal{F} + \frac{\rho_0^2}{E_0} \alpha_t \Gamma_t \partial_t^2 \mathcal{F} - \rho_0 (1 + \alpha_x) \Gamma_x \partial_x^2 \mathcal{F}.
 \end{aligned}$$

The high-order wave equation (62) is formally identical to that given by the
 stress gradient model in (49). This legitimates the stress gradient model as
 a candidate for the effective description of heterogeneous media in the low
 frequency range. Identification of the terms between (62) and (49) leads to

the following relations, with the superscript \dagger on stress gradient parameters:

$$U^\dagger = \mathcal{U}, \quad F_U^\dagger = \mathcal{F}, \quad F_\zeta^\dagger = \frac{\mathcal{F}}{\alpha_t}, \quad (63a)$$

$$\varrho^\dagger = \rho_0, \quad E^\dagger = E_0, \quad (63b)$$

$$B^\dagger = \Gamma_x + \Gamma_t, \quad D^\dagger = \frac{E^\dagger}{B^\dagger} = \frac{E_0}{\Gamma_x + \Gamma_t}, \quad (63c)$$

$$b_x^{\dagger 2} = \alpha_x \Gamma_x, \quad \kappa^\dagger = E^\dagger \frac{b_x^{\dagger 2}}{B^\dagger} = E_0 \frac{\alpha_x \Gamma_x}{\Gamma_x + \Gamma_t}, \quad (63d)$$

$$b_t^{\dagger 2} = \alpha_t \Gamma_t, \quad \mu^\dagger = \varrho^\dagger \frac{b_t^{\dagger 2}}{B^\dagger} = \rho_0 \frac{\alpha_t \Gamma_t}{\Gamma_x + \Gamma_t}, \quad (63e)$$

$$b_m^{\dagger 2} = (1 + \alpha_x) \Gamma_x + (1 + \alpha_t) \Gamma_t = B^\dagger + b_x^{\dagger 2} + b_t^{\dagger 2}. \quad (63f)$$

323 All the families of models defined through (62) share the same degree of
 324 asymptotic accuracy. They all have the same density ϱ^\dagger , elasticity modulus
 325 E^\dagger and stress gradient coefficient B^\dagger , defined without ambiguity by homog-
 326 enization, independently of the coefficients α_x and α_t . As a consequence
 327 of (35) where only ϱ^\dagger , E^\dagger and B^\dagger are involved, the dispersion relations of
 328 all models are therefore asymptotically the same at low frequencies. This
 329 implies that discrimination between auxiliary inertia (weighted by α_t) and
 330 auxiliary elasticity (weighted by α_x) in micro-structural effects can be made
 331 only at higher frequencies.

332 The orders of magnitude for coefficients α_t and α_x are constrained by
 333 asymptotic homogenization, which requires that $\epsilon^2 \mathcal{C}_2^{(2)}(\mathcal{U}^{(0)})$ remains a cor-
 334 rector of order ϵ^2 in (58). It results in the orders of magnitude $\alpha_t = \mathcal{O}(\epsilon^m)$
 335 and $\alpha_x = \mathcal{O}(\epsilon^m)$ with integer $m \geq 0$.

336 *4.3. Closing criteria from Bloch-Floquet analysis*

337 As analysed in Sec 2, the parameters B^\dagger , b_t^\dagger and b_x^\dagger are required to be
 338 positive. We assume that asymptotic homogenization theory provides $B^\dagger >$
 339 0. This property is confirmed numerically through multiple configurations
 340 tested in Sec. 5, even if it remains to be proven rigorously.

341 Various closing criteria for b_t^\dagger and b_x^\dagger can be found in the literature in
 342 other contexts [36, 11, 14], mostly related to bilaminate micro-structures.
 343 Examples of such closing criteria are recalled in Sec. 5.1, where the study case
 344 of bilaminate micro-structures is revisited for comparison with the closing
 345 criteria that we choose here.

346 Our criteria follows the same aim of global fit as in [36, 11, 14] but is
 347 defined so that it can be applied to any 1-D periodic architecture, while
 348 positivity constraints $b_t^\dagger > 0$ and $b_x^\dagger > 0$ are satisfied: we choose to define
 349 b_t^\dagger and b_x^\dagger as the strictly-positive parameters which minimize the difference
 350 between the dispersion relations computed from the stress gradient model
 351 and Bloch-Floquet calculations on the heterogeneous medium.

352 In Bloch-Floquet calculations on the heterogeneous 1-D periodic medium,
 353 the dispersion relation is obtained numerically after substitution of the ansatz
 354 $u(x) = \eta(x) \exp(ikx - i\omega t)$ into the governing equations (50), yielding the
 355 eigenvalue problem,

$$356 \quad \omega^2 \rho \eta + \partial_x \{ a \partial_x \eta + ik a \eta \} + ik a \partial_x \eta - k^2 a \eta = 0, \quad (64)$$

357 where the cell function $\eta(x)$ is periodic. Then, the parameters b_t^\dagger and b_x^\dagger are
 358 obtained through the minimisation

$$359 \quad (b_t^\dagger, b_x^\dagger) = \underset{b_t^*, b_x^* > 0}{\operatorname{argmin}} \Phi(b_t^*, b_x^*), \quad (65)$$

360 where the deviation function Φ reads

$$361 \quad \Phi(b_t^*, b_x^*) = \frac{1}{N} \sqrt{\sum_{m=1}^{m=N} |\omega_m^I - \bar{\omega}_+^I(k_m, b_t^*, b_x^*)|^2}. \quad (66)$$

362 The angular frequencies ω_m^I denote the lowest eigenvalues of the problem
 363 stated in (64) for given values of the wavenumber $k = k_m = m\pi/(N\ell)$ with
 364 integers $1 \leq m \leq N$ and $N \geq 2$. The angular frequencies $\bar{\omega}_+^I(k_m, b_t^*, b_x^*)$
 365 defined in (39) are computed at wavenumber k_m for the stress gradient ma-
 366 terial having inner-lengths b_t^* and b_x^* , with parameters ϱ^\dagger , E^\dagger , and B^\dagger given
 367 by asymptotic homogenization. In (65), the minimum of the deviation func-
 368 tion is found by means of the Nelder-Mead Simplex Method [37] using the
 369 routine `fminsearch` in commercial software MatLab, with added bounds
 370 $b_t^*, b_x^* \in]0, 10\ell]$.

371 This numerical procedure enforces the strict positivity of b_t^\dagger and b_x^\dagger , ensur-
 372 ing the hyperbolicity and stability of the model. It can be applied to any 1-D
 373 unit cell Ω , whether layered or continuously graded. Once the parameters b_t^\dagger
 374 and b_x^\dagger are obtained from the minimisation in (65), the coefficients α_x and α_t
 375 can be calculated according to (63d) and (63e), and the auxiliary bulk force
 376 F_ζ^\dagger is determined by (63a).

377 5. Numerical applications

378 In this section, the micro-macro procedure presented in previous Sec. 4
 379 is applied. The objectives developed in the numerical applications are three-
 380 fold. First, the influence of the choice in the closing criteria is illustrated
 381 in Sec. 5.1. To this aim, our closing criteria is compared to those proposed

382 by Wautier & Guzina [11] or Cornaggia & Guzina [14] in 1-D periodic bi-
383 laminate micro-structures. Second, a parametric study on values of param-
384 eters for multi-laminate materials with up to 10 layers in the unit cell is
385 performed in Sec. 5.2. This led us to evidence the range of values for the
386 stress gradient parameters, and their respective influence over dispersion re-
387 lations. Finally, in Sec. 5.3, transient time-domain calculations are performed
388 in response to oscillatory bulk forces in both multi-laminate periodic media
389 and corresponding stress gradient media. They evidence the benefits of the
390 equivalent continuum descriptions.

391 5.1. Comparison of closing criteria in bi-laminate materials

392 The micro-structure consists of the 1-D periodic repetition of the ℓ -sized
393 unit cell Ω made of the two homogeneous elastic layers $\Omega^{[1]}$ and $\Omega^{[2]}$ having
394 the thickness $\ell^{[1]} = \phi^{[1]}\ell$ and $\ell^{[2]} = \phi^{[2]}\ell = (1 - \phi^{[1]})\ell$, densities $\rho^{[1]}$ and
395 $\rho^{[2]}$, local elastic moduli $a^{[1]}$ and $a^{[2]}$, and wave speeds $c^{[1]} = \sqrt{a^{[1]}/\rho^{[1]}}$ and
396 $c^{[2]} = \sqrt{a^{[2]}/\rho^{[2]}}$. As detailed in Appendix B.2, closed-form formula can
397 be derived for the effective material properties in bilaminate structures. In
398 particular, the stress gradient parameter is shown to be positive, $B^\dagger > 0$,
399 which is essential for energy consistency of the stress gradient model, see
400 Sec. 2.

401 We consider the same micro-structure used by Wautier & Guzina [11],
402 with normalised parameters

$$403 \quad \phi^{[1]} = \phi^{[2]} = \frac{1}{2}, \quad \frac{\rho^{[2]}}{\rho^{[1]}} = 0.6, \quad \frac{a^{[2]}}{a^{[1]}} = 0.4, \quad (67)$$

which lead to the effective material parameters according to [Appendix B.2](#)

$$\frac{\rho_0}{\rho^{[1]}} = 0.8, \quad \frac{E_0}{a^{[1]}} \approx 0.571, \quad \frac{B^\dagger}{\ell^2} \approx 9.593 \times 10^{-3}, \quad (68a)$$

$$\frac{\Gamma_x}{B^\dagger} \approx 0.233, \quad \frac{\Gamma_t}{B^\dagger} \approx 0.767. \quad (68b)$$

404 We compare our results with those obtained in [14] and [11] with different
 405 closing criteria. Using the high-order continuum model (62) with $b_x^\dagger \equiv 0$ to
 406 describe a bilaminate without bulk force, Cornaggia & Guzina [14] fixed the
 407 value of b_t^\dagger by equating the terms up to $(k_0\ell)^5$ in the Taylor expansions of the
 408 dispersion relation in the high-order continuum model and in the bilaminate
 409 material. Doing so resulted into the closed-form formula for squared inner-
 410 lengths, denoted with CG as superscript,

$$411 \quad \begin{cases} (b_x^{\text{CG}})^2 &= 0, \\ (b_t^{\text{CG}})^2 &= (\ell^2 - 6B^\dagger - 4J^{\text{CG}})/10, \\ (b_m^{\text{CG}})^2 &= B^\dagger + (b_x^{\text{CG}})^2 + (b_t^{\text{CG}})^2, \end{cases} \quad (69)$$

412 where the characteristic surface J^{CG} is given by

$$413 \quad J^{\text{CG}} = \frac{\ell^2}{12} \left(\left(\phi^{[1]} \frac{c_0}{c^{[1]}} \right)^2 - \left(\phi^{[2]} \frac{c_0}{c^{[2]}} \right)^2 \right)^2. \quad (70)$$

414 The closing criteria (69) with $b_x^{\text{CG}} = 0$ results into the original stress gradient
 415 model. Using micro-structure described in Eq. (67) the values found for the
 416 squared inner-lengths and resulting material parameters are given in Tab. 1.

417 In another study on high-order continuum model (62) applied to describe
 418 the bilaminate micro-structure without bulk force, Wautier & Guzina [11]
 419 used all three inner lengths (b_x , b_t , b_m) along with the relation (15) and the
 420 following closing criteria: (i) the group velocity $d\omega/d(\text{Re}(k))$ at the end of

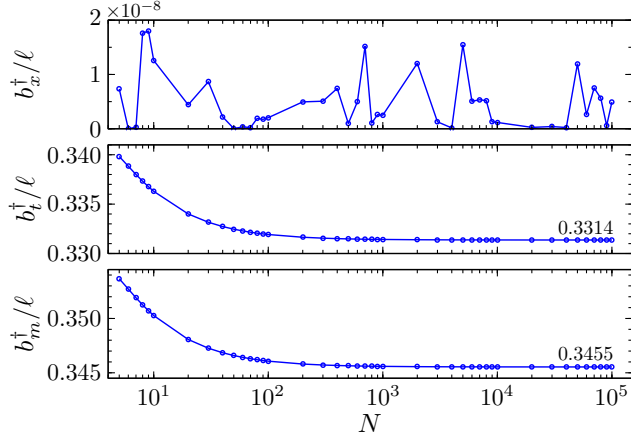


Figure 3: Values of normalised inner-lengths issued from closing criterion (65) with the number N of Bloch wavenumbers used for minimisation for 1-D periodic bilaminate materials described in (68).

421 the Brillouin zone $\text{Re}(k\ell) = \pi$ is zero; and (ii) the frequency-jump in the
 422 dispersion relation between branches $\text{Re}(k^{\text{I}})$ and $\text{Re}(k^{\text{II}})$ of the stress gradient
 423 model at the end of the Brillouin zone $\text{Re}(k\ell) = \pi$ equals the frequency
 424 bandwidth of first Bragg bandgap in bilaminate materials. The approach is
 425 numerical, and leads to values of inner-lengths b_x^{WG} , b_t^{WG} , b_m^{WG} and weighting
 426 factors α_x^{WG} and α_t^{WG} given in Tab. 1, and denoted with the superscript
 427 WG. However, such conditions led to the purely imaginary inner-length
 428 $b_x^{\text{WG}} \approx 0.2252i$, which implies the negative auxiliary elasticity modulus $\kappa^\dagger =$
 429 $E(b_x^{\text{WG}})^2/B^\dagger < 0$, making the model energetically inconsistent and unstable,
 430 see Sec. 2.

431 Finally, the criteria (65) proposed here is used. The eigenvalue problem
 432 (64) related to Bloch-Floquet analysis is solved numerically by the Plane
 433 Wave Method presented in Appendix C. Fig. 3 shows the values of normalised
 434 inner-lengths issued from closing criterion using different number N of Bloch

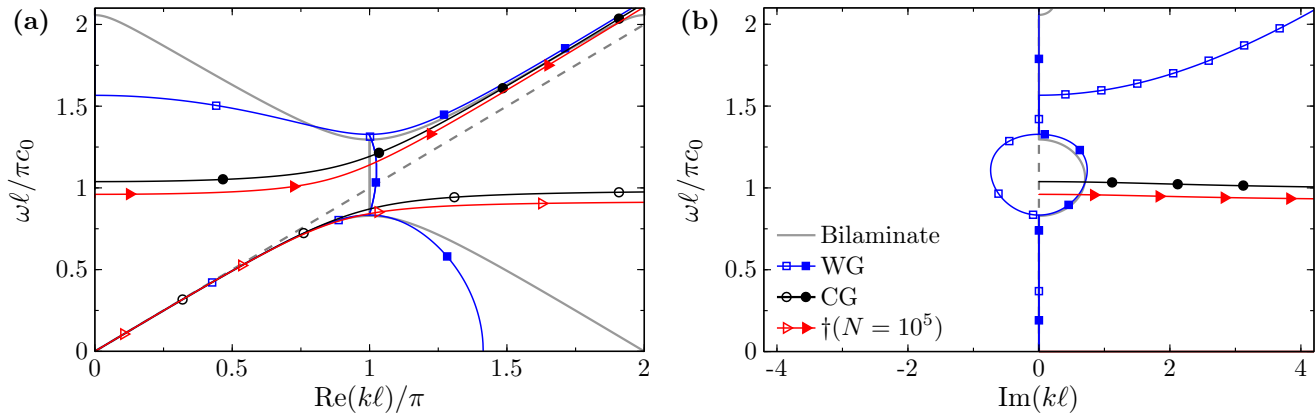


Figure 4: (Color online) Dispersion relation with (a) real and (b) imaginary parts of normalised wavenumbers versus normalised frequency in 1-D periodic bilaminate materials described in Eq. (68) and its stress gradient continuum representations using closing criteria WG, CG, and †, defined by Wautier & Guzina [11], Cornaggia & Guzina [14], and in the present work (with $N = 10^5$ Bloch wavenumbers used in minimisation) respectively. Here, filled or empty symbols stand for different modes. Dashed grey line corresponds to elastodynamic relation $k = \omega/c_0$. For clarity, branches which satisfy $\text{Im}(k) = 0$ have not been represented in Fig. (b), except for WG calculations.

	WG	CG	† ($N = 10^5$)	† ($N = 20$)
b_x^*/ℓ	0.2252 i	0	4.93×10^{-9}	4.41×10^{-9}
b_t^*/ℓ	0.2032	0.3066	0.3314	0.3340
b_m^*/ℓ	0.0139	0.3218	0.3455	0.3481
α_x^*	-22.71	0	1.09×10^{-14}	8.72×10^{-15}
α_t^*	5.61	12.77	14.9174	15.1558

Table 1: Values of normalised inner-lengths (b_x^* , b_t^* , b_m^*)/ ℓ , and weighting factors (α_x^* , α_t^*) following closing criteria WG, CG, and †, defined by Wautier & Guzina [11], Cornaggia & Guzina [14], and in the present work (with $N = 10^5$ or $N = 20$ Bloch wavenumbers used in minimisation) respectively. Calculations performed for micro-structure given in Eq. (67).

435 wavenumbers in minimisation. For $N = 20$, the inner lengths b_t^\dagger and b_m^\dagger
436 already reached the value obtained for $N = 10^5$ with less than 1% error. On
437 the other hand, the smallness of the inner length b_x^\dagger compared to the two
438 other inner-length, and its difficulty to converge towards a definite value, are
439 noticeable. This difficulty might be due to the low sensitivity of the acoustic
440 branch of the dispersion relation (on which is performed the minimisation)
441 on b_x^\dagger . Values of inner-lengths and weighting factors for $N = 10^5$ and $N = 20$
442 are reported in Tab. 1.

443 Fig. 4 displays the dispersion relations for the 1-D periodic bilaminate
444 material, and for the stress gradient media with parameters issued from WG
445 and CG criteria, and from our closing criterion (65). Focusing only on the
446 real part of the wavenumbers in Fig. 4(a), all stress gradient representation
447 are in excellent agreement with the acoustic branch of the dispersion relation
448 of the bilaminate material in the first Brillouin zone $\text{Re}(k\ell) \leq \pi$. However,

449 for larger wavenumbers and higher frequencies outside this zone, the stress
 450 gradient continuum is inaccurate in its representation of the bilaminate ma-
 451 terial (for all closing criteria), and remains therefore a long-wavelength/low-
 452 frequency effective medium.

453 Despite their irrelevance at high frequencies, the continuum models must
 454 remain stable. Here, the imaginary part of the wavenumbers represented in
 455 Fig. 4(b) reveals clearly that stress gradient medium using the WG closing
 456 criterion is unstable: in the vicinity of the Bragg limit $\text{Re}(k\ell) \equiv \pi$, the imag-
 457 inary part of the wavenumber becomes negative, which results in displace-
 458 ments that increase exponentially as they propagate. Finally, using $N = 10^5$
 459 or $N = 20$ Bloch wavenumbers in our closing criterion (65) produces no
 460 significant effects upon the dispersion relation (graphically superimposed) in
 461 the long-wavelength/low-frequency range wherein stress gradient continuum
 462 is relevant.

463 5.2. Parametric study on multi-laminate materials

464 The proposed closing criterion (65) can be applied to any 1-D periodic
 465 micro-structure to retrieve both positive inner-lengths b_t^\dagger and b_x^\dagger . An heuristic
 466 study on 1-D periodic multi-laminate materials is then conducted so as to
 467 evidence ranges of values for effective stress gradient parameters.

468 The 1-D periodic multi-laminate material consists of the ℓ -sized unit cell Ω
 469 made of the $n = 1 \dots \mathcal{N}$ homogeneous elastic layers $\Omega^{[n]} = [L^{[n]}, L^{[n+1]}]$ having
 470 the densities $\rho^{[n]}$, local elastic moduli $a^{[n]}$, and thickness $\ell^{[n]} = L^{[n+1]} - L^{[n]}$.
 471 Closed-form formula for effective material parameters ρ_0 , E_0 , h , Γ_x , Γ_t and B^\dagger
 472 in 1-D periodic multi-laminate materials are derived in [Appendix B](#) according
 473 to (56) by solving the cell problems (57) .

474 The micro-structural parameters $\ell^{[n]}$, $\rho^{[n]}$, and $a^{[n]}$ are chosen in the form
 475 10^v , where v is a number picked randomly in the interval $[-1.2, 1.2]$ according
 476 to the uniform law. The effective material parameters ρ_0 , E_0 , h , Γ_x , Γ_t
 477 and B^\dagger are computed according to [Appendix B](#). The closing criterion (65)
 478 with 20 Bloch wavenumbers is used to derive the stress gradient continuum
 479 corresponding to the multi-laminate material. Such systematic procedure
 480 is applied for micro-structures with $\mathcal{N} = 2, 3, 5$, and 10 layers in the unit
 481 cell, and 10 000 random realisations of micro-structures is considered for each
 482 number \mathcal{N} . Figure 5 shows the histogram (or distribution density) of values
 483 reached by the parameters once normalised by ℓ , ρ_0 or E_0 .

484 Values reached by micro-structural parameters $\ell^{[n]}/\ell$, $\rho^{[n]}/\rho_0$, and $a^{[n]}/E_0$,
 485 cover nearly 3 orders of magnitudes each. As for material parameters issued
 486 from two-scale asymptotic homogenization, Γ_x/ℓ^2 and h/ℓ can reach posi-
 487 tive and negative values, while Γ_t/ℓ^2 and B^\dagger/ℓ^2 are always positive. As for
 488 inner-lengths, results show that the approximation $b_t/\ell \approx 1/3$ is relevant for
 489 all realisations of micro-structures considered here, while b_x remains much
 490 smaller than b_t with $b_x/\ell \sim 5 \times 10^{-9}$ and the approximation $b_x/\ell = 0$ is
 491 tantalizing. The inner-length $b_m = \sqrt{B + b_x^2 + b_t^2}$ and weighting coefficients
 492 $\alpha_x = b_x^2/\Gamma_x$ and $\alpha_t = b_t^2/\Gamma_t$ are then obtained from the other parameters,
 493 and their range of values is given for illustration.

494 5.3. Time-domain simulations

495 Finally, time-domain simulations are performed on a 1-D periodic tri-
 496 laminate material and its equivalent stress gradient continuum. Micro-structural

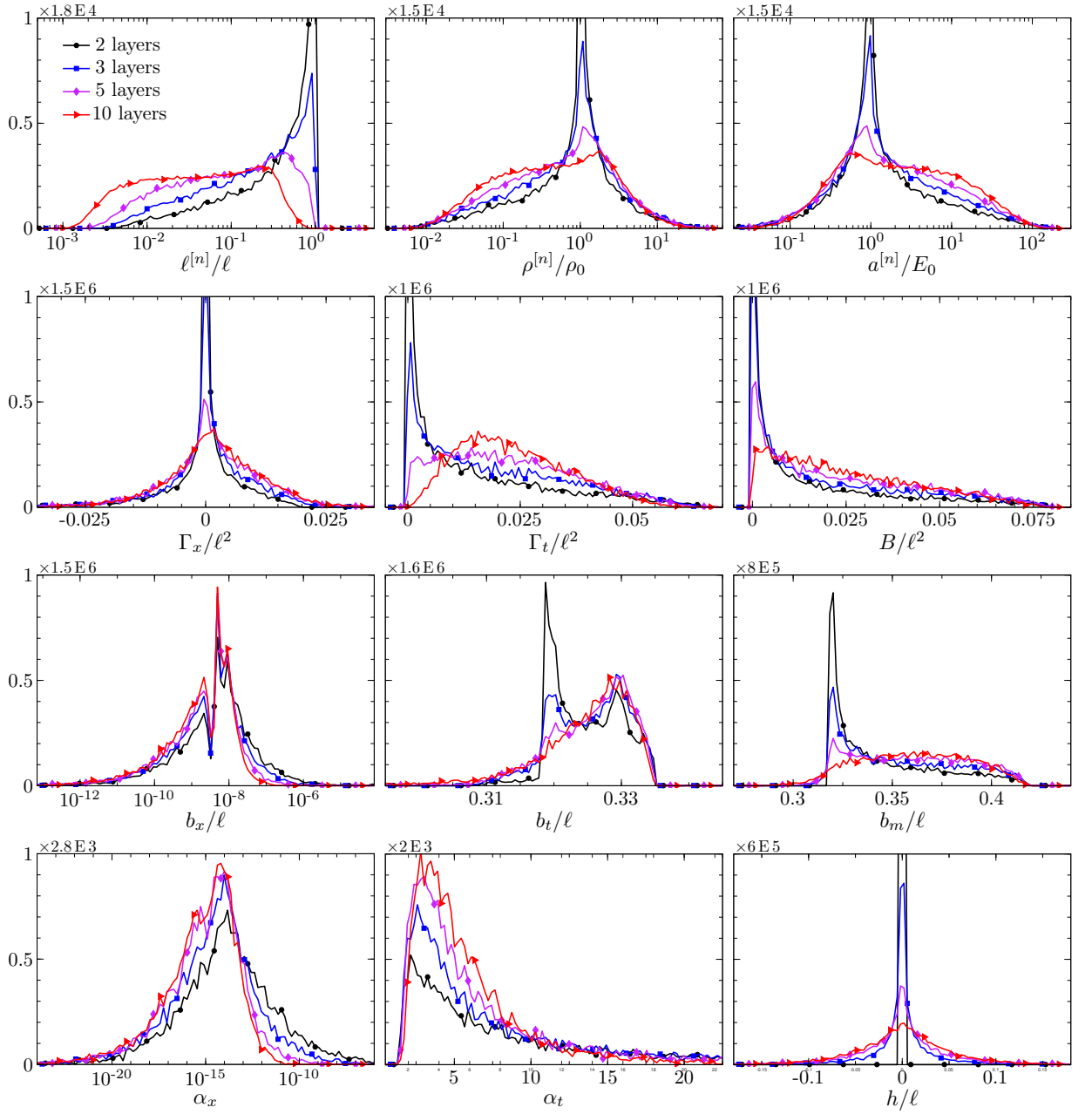


Figure 5: (Color online) Histogram (or distribution density) of characteristic parameters for random realisations of 1-D periodic multi-laminate materials with $\mathcal{N} = 2, 3, 5$ and 10 layers in the unit cell. For each number \mathcal{N} of layers, 10 000 random realisations are considered.

497 parameters for the tri-laminate material are chosen according to

$$\left. \begin{aligned}
 &\ell^{[1]} = 0.3 \ell, & \ell^{[2]} = 0.3 \ell, & \ell^{[3]} = 0.4 \ell, \\
 &a^{[1]} = 0.45 E_0, & a^{[2]} = 3.90 E_0, & a^{[3]} = 1.56 E_0, \\
 &\rho^{[1]} = 0.34 \rho_0, & \rho^{[2]} = 0.14 \rho_0, & \rho^{[3]} = 2.14 \rho_0,
 \end{aligned} \right\} \quad (71)$$

499 which lead to the normalised parameters

$$\left. \begin{aligned}
 &\Gamma_x/\ell^2 \approx 0.009, & \Gamma_t/\ell^2 \approx 0.022, & B^\dagger/\ell^2 \approx 0.032, \\
 &b_x^\dagger/\ell \approx 5 \times 10^{-9}, & b_t^\dagger/\ell \approx 0.33, & b_m^\dagger/\ell \approx 0.38, \\
 &\alpha_x \approx 3 \times 10^{-15}, & \alpha_t \approx 4.92, & h/\ell \approx -0.07.
 \end{aligned} \right\} \quad (72)$$

501 Dimensional parameters are used, with the period size $\ell = 40$ m, the density
 502 $\varrho = \rho_0 = 2980$ kg/m³, and the elasticity modulus $E = E_0 = 2.33 \times 10^9$ Pa.
 503 Using (63), it yields the auxiliary density $\mu \approx 3.5 \rho_0 \approx 10358$ kg/m³, the
 504 auxiliary elasticity modulus $\kappa \approx 2.2 \times 10^{-6}$ Pa $\ll E_0$, and the stress gradient
 505 modulus $D \approx 4.6 \times 10^7$ Pa/m². The dispersion relations in the 1-D periodic
 506 tri-laminate material and its equivalent stress gradient continuum are shown
 507 in Fig. 6. The straight line $k = \omega/c_0$ corresponding to the non-dispersive
 508 Cauchy medium with density ϱ and elasticity modulus E is also plotted.

509 The medium $x \in [0, L]$ is $L = 2000$ m long and consists of 50 unit
 510 cells, with abscissa $x = L/2$ corresponding to the interface between $\Omega^{[3]}$ at
 511 $x = (L/2)^-$ and $\Omega^{[1]}$ at $x = (L/2)^+$.

512 Whether in the tri-laminate materials, or its equivalent stress gradient and
 513 Cauchy continua, a uniform Cartesian grid with mesh size δx and time step
 514 δt is introduced. A fourth-order ADER scheme is implemented to integrate
 515 the evolution equations [38]. This explicit two-step and single-grid finite-
 516 difference scheme is stable under the usual CFL condition:

$$\nu = \max(c_i) \frac{\delta t}{\delta x} \leq 1, \quad (73)$$

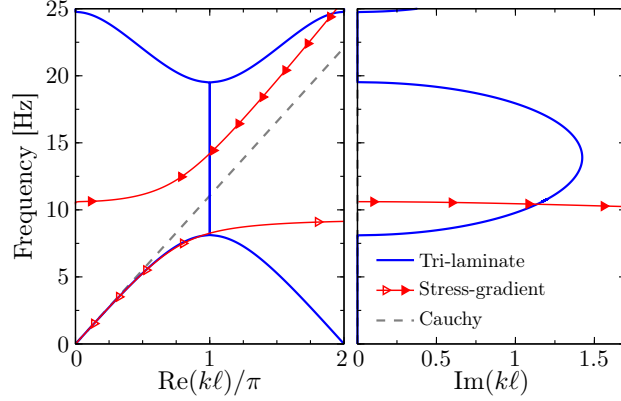


Figure 6: (Color on-line) Complex dispersion relation in the 1-D tri-laminate material described in Eq. (71), and in its equivalent stress gradient and Cauchy media characterised by parameters $(\varrho, E, \mu, \kappa, D)$ and (ϱ, E) respectively. See main text for values.

518 where c_i is the maximal eigenvalue of \mathbb{A} at node i . In multi-laminate materi-
 519 als, a large number of interfaces is involved. To ensure a correct discretisation
 520 of the jump conditions, and hence to provide reliable reference solutions, we
 521 implement an immersed interface method [39]. While the relaxation matrix
 522 \mathbb{S} is null in Cauchy media, \mathbb{S} is non-null in equivalent stress gradient media.
 523 Its contribution is then discretised by a splitting approach [40]. In what fol-
 524 lows, the spatial mesh size is $\delta x = 1$ m and the time step is deduced from
 525 the CFL condition (73) where $\nu = 0.95$ is chosen.

526 The following external force is considered

$$527 \quad f(x, t) = X_f(x) \mathcal{T}_f(t). \quad (74)$$

The time and space functions $\mathcal{T}_f(t)$ and $X_f(x)$ read

$$\mathcal{T}_f(t) = \sum_{m=1}^4 \mathbb{1}_{[0, T_c]} \hat{f}_m \sin(2^{m-1} \omega_c t), \quad (75a)$$

$$X_f(x) = \exp(-x^2/(2d^2)). \quad (75b)$$

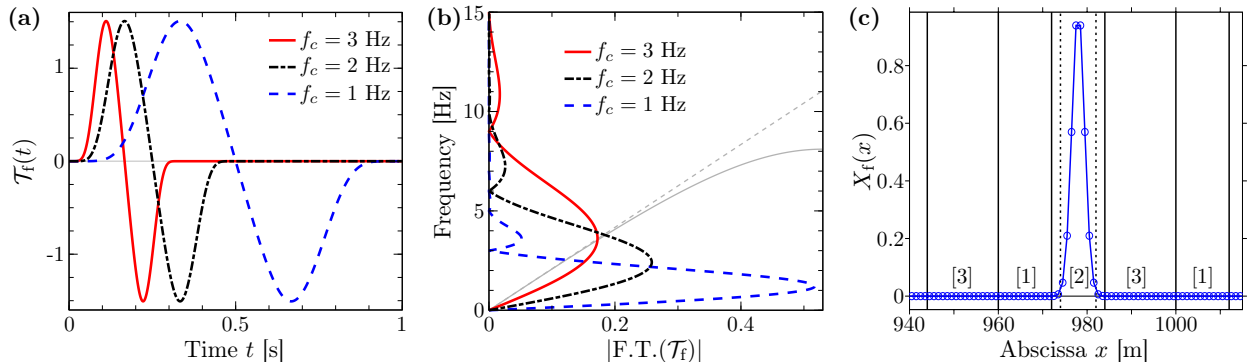


Figure 7: (Color on-line) External bulk force applied to materials in time-domain calculations. (a) Time signals $\mathcal{T}_f(t)$ for three central frequencies f_c ; (b) Fourier Transform (F.T.) of time signals $\mathcal{T}_f(t)$; and (c) space function $X_f(x)$ applied in the phase $\Omega^{[2]}$ in vicinity of central abscissa $x_s = 978$ m. In figure (b), the shapes of dispersion relations for 1-D periodic tri-laminate material and its equivalent Cauchy medium are plotted in thin continuous and dashed grey lines respectively.

528 In (75a), the time function $\mathcal{T}_f(t)$ is a combination of sinusoids with support
529 bounded to the time interval $t \in [0, T_c]$ by the indicator function $\mathbb{1}_{[0, T_c]}$
530 equal to 1 over $[0, T_c]$ and 0 elsewhere. The amplitudes of the sinusoids
531 are $\hat{f}_1 = 1$, $\hat{f}_2 = -21/32$, $\hat{f}_3 = 63/768$ and $\hat{f}_4 = -1/512$. It makes the dif-
532 ferentiability class of time function $\mathcal{T}_f(t)$ of order 6, which enable the use
533 of numerical scheme ADER 4 [41] for time-domain calculations. The time
534 evolution of $\mathcal{T}_f(t)$ and its frequency spectrum are displayed in Fig. 7(a) and
535 (b). In particular, Fig. 7(b) shows that $\mathcal{T}_f(t)$ is a broadband signal with de-
536 creasing spectral lobes, the first principal lobe having the central frequency
537 $f_c = 1/T_c = \omega_c/2\pi$. The values $f_c = \{1; 2; 3\}$ Hz are considered, correspond-
538 ing to scale factors $\epsilon_c = \ell\omega_c/c_0 = \{0.28; 0.57; 0.85\}$. While most frequency
539 content of signal with central frequency $f_c = 1$ Hz is within the low frequency

540 range, the whole acoustic branch of the dispersion relation related to the tri-
 541 laminate material is excited for central frequency $f_c = 3$ Hz (and its second
 542 lobe is within first Bragg bandgap).

543 In (75b), the space function $X_f(x)$ is a Gaussian function centred at $x_s =$
 544 978 m (phase $\Omega^{[2]}$ in the tri-laminate material) and with standard deviation
 545 $d = 4/\sqrt{2} \approx 2.83$ m, see Fig. 7(c). The Gaussian is actually cancelled at grid
 546 nodes x_i such that $|x_i - x_s| \geq 2d$, which makes the source terms belong only to
 547 the phase $\Omega^{[2]}$ in the tri-laminate material. Using micro-macro relations (63a)
 548 with (59b), the external bulk force F_U^\dagger applied in stress gradient medium and
 549 corresponding to (74) reads

$$550 \quad F_U^\dagger(x, t) = \left[1 + \frac{h}{d} \frac{x}{d} + \frac{h^2}{d^2} \left(\frac{x^2}{d^2} - 1 \right) \right] f(x, t). \quad (76)$$

551 The forces F_U^\dagger and F_ζ^\dagger in the equivalent stress gradient medium are applied
 552 at the same nodes x_i as in the tri-laminate material.

553 Figure 8 shows the particle velocity $\partial_t u$ in the tri-laminate material, and
 554 v in its equivalent stress gradient and Cauchy media, at $t = 1$ s. For central
 555 frequency $f_c = 1$ Hz, the dispersive effects are negligible, and the agreement
 556 of both stress gradient and Cauchy models (leading-order homogenization)
 557 with reference field in tri-laminate material is excellent. The interest of
 558 the stress gradient model occurs at higher frequencies, when the dispersive
 559 effects are solicited: at $f_c = 2$ Hz, the oscillations are well captured by the
 560 stress gradient model and the amplitude of the waves is also reproduced. At
 561 $f_c = 3$ Hz, the stress gradient model remains still in good agreement with the
 562 reference signal in tri-laminate material, while severe discrepancies in terms
 563 of wave dispersion and amplitudes can be observed for the Cauchy medium.
 564 Near the source, at $f_c = 2$ Hz and $f_c = 3$ Hz, a sharp peak in the velocity is

565 due to the small support of the source, included within one micro-structural
566 layer: it disappears when we spread the source by increasing d (not shown
567 here).

568 Hence, even under poor condition of scale separation ($\epsilon_c = 0.85$ for central
569 frequency $f_c = 3$ Hz) and for an external bulk source with micro-structural
570 support, the stress gradient model remains robust to capture the dispersive
571 size effects within the micro-structured material, at small distance away from
572 the zone where the force is applied. All the results presented in Fig. 8 are
573 given with the same number of nodes for both the 1-D periodic tri-laminate
574 material and the homogeneous equivalent media. In the low-frequency range,
575 this number of nodes is mostly driven by the discretisation of the micro-
576 structural layers in the tri-laminate material. This constraint is obviously not
577 present in the homogeneous equivalent media and a $1/\epsilon$ -coarser mesh would
578 be sufficient to compute fields with an accuracy nearly as good. In addition, a
579 coarser mesh lowers also the number of time-steps through the CFL condition
580 (73). These aspects emphasise the high interest of homogenization models
581 in dynamic simulations.

582 Figure 9 shows the snapshots of the elastic and auxiliary velocities v and
583 φ in the case $f_c = 1$ Hz. It evidences that (i) in the low-frequency range
584 where the stress gradient model is relevant, the auxiliary velocity φ is much
585 smaller than elastic velocity v , by two orders of magnitude here; and (ii) φ
586 is a long-wavelength field with spatial variations as large as v , and is not a
587 micro-structural field with period-wise variations.

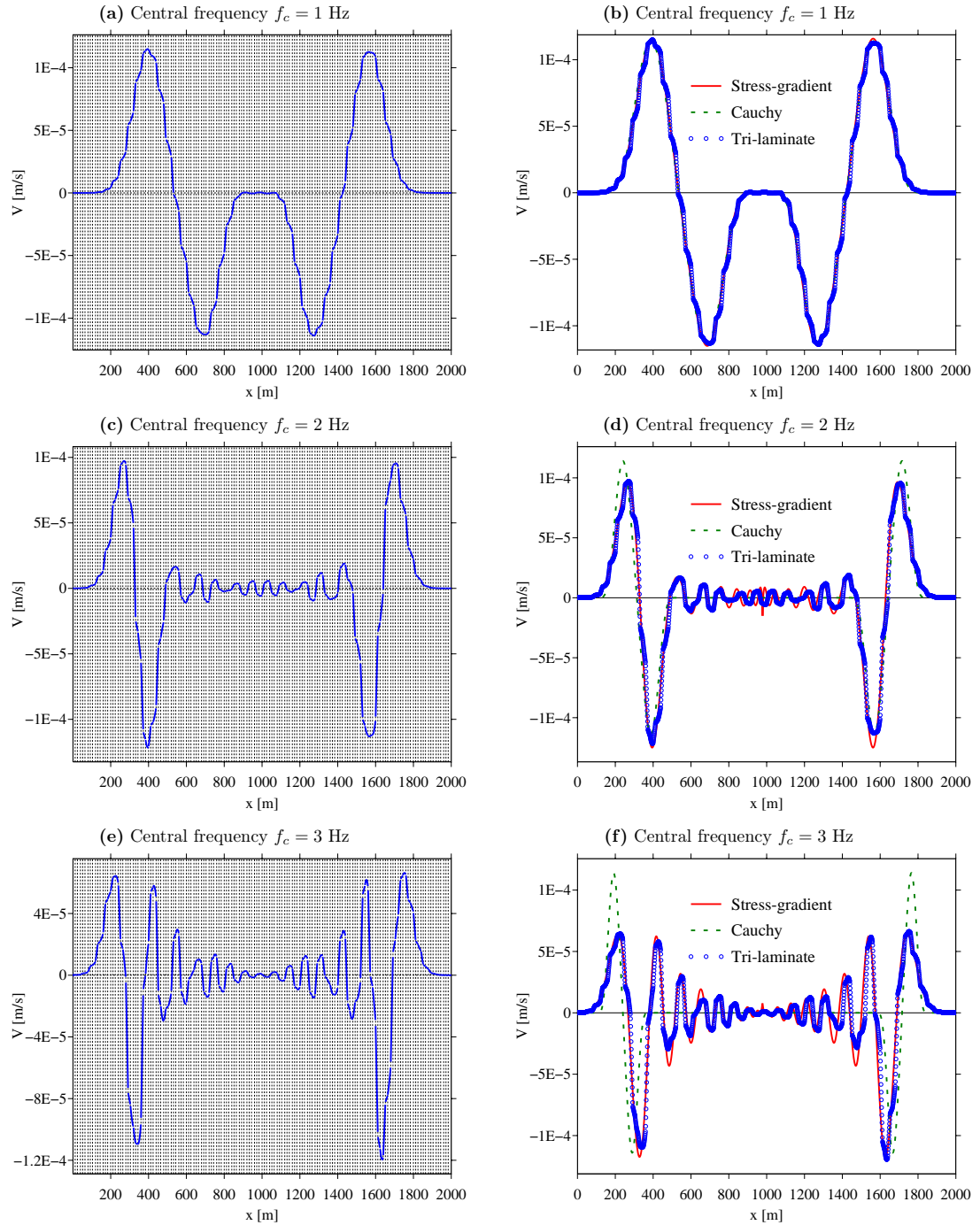


Figure 8: (Color online) Snapshot at $t = 1$ s of the elastic velocity emitted by a source at $x_s = 978$ m (phase $\Omega^{[2]}$ in the tri-laminate material) for various central frequencies f_c : 1 Hz ($\epsilon_c = 0.28$), 2 Hz ($\epsilon_c = 0.57$) and 3 Hz ($\epsilon_c = 0.85$). Left: Elastic velocity in the 1-D periodic tri-laminate material. Right: comparison between fields in 1-D periodic tri-laminate material and its equivalent stress gradient Cauchy homogeneous media.

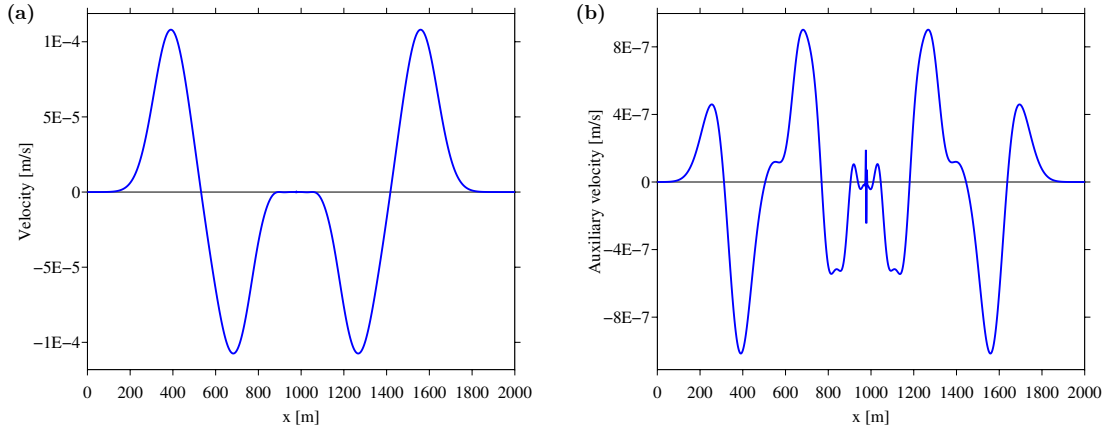


Figure 9: (Color online) Snapshot at $t = 1$ s of the elastic velocity v in (a) and auxiliary velocity φ in (b) emitted by a source at $x_s = 978$ m for $f_c = 1$ Hz.

588 6. Conclusions

589 This paper focused on the dynamic study of stress gradient materials in
 590 1D. For generality, an extended stress-gradient model was considered, intro-
 591 ducing an additional inner-length to the original stress gradient model and a
 592 term in ∂_x^4 in the wave equation. On the one hand, we studied theoretically
 593 the properties of waves in the extended model: hyperbolicity, stability, dis-
 594 persion and causality. On the other hand, we proposed a numerical method
 595 to identify the parameters of this model to represent the dynamic behavior
 596 of a microstructured Cauchy medium. The numerical experiments showed
 597 that the dispersive effects were then well captured by the homogeneous stress
 598 gradient material. A systematic numerical study showed that the additional
 599 parameter of the extended model was very close to 0 when it comes to repre-
 600 sent classical heterogeneous elastic media, and could very well be neglected
 601 in that case. Contrary to a usually-accepted postulate, this parameter is not

602 necessary for causality. An interesting perspective of this work concerns the
603 study (theoretical and numerical) of stress gradient media in higher spatial
604 dimensions.

605 **Acknowledgments**

606 This research has been supported by Labex MEC *Mécanique et Com-*
607 *plexité*, Initiative d'Excellence A*MIDEX, Investissements d'Avenir. B Lom-
608 bard thanks S. Forest for drawing his attention to the study of wave prop-
609 agation in stress gradient media. L. Schwan is grateful to R. Cornaggia for
610 fruitful discussions.

611 **Appendix A. Two-scale asymptotic homogenization**

This appendix describes the two-scale asymptotic homogenization high-order terms. The approach follows the procedure developed initially in 3-D elastodynamics without bulk force [20] or 3-D elastostatics with the bulk force [19, 21], and applied in more recent work [13, 11, 14] in 1-D elastodynamics without bulk force f . Here, the problem in elastodynamics with the mass density of external bulk force f is tackled. After substitution of asymptotic expansions (52) into governing equations (50) expressed with two-scale differential operator $\partial_x + \epsilon^{-1}\partial_y$, terms of equal power of ϵ are collected to

provide

$$\partial_y u^{(0)} = 0, \tag{A.1a}$$

$$\partial_y s^{(0)} = 0, \tag{A.1b}$$

$$s^{(0)} = a(\partial_y u^{(1)} + \partial_x u^{(0)}), \tag{A.1c}$$

$$\partial_y s^{(1)} + \partial_x s^{(0)} = \rho(\partial_t^2 u^{(0)} - f), \tag{A.1d}$$

$$s^{(1)} = a(\partial_y u^{(2)} + \partial_x u^{(1)}), \tag{A.1e}$$

$$\partial_y s^{(2)} + \partial_x s^{(1)} = \rho \partial_t^2 u^{(1)}, \tag{A.1f}$$

$$s^{(2)} = a(\partial_y u^{(3)} + \partial_x u^{(2)}), \tag{A.1g}$$

$$\partial_y s^{(3)} + \partial_x s^{(2)} = \rho \partial_t^2 u^{(2)}. \tag{A.1h}$$

612 First, y -averaged values $\mathcal{U}^{(j)}(x)$ and $\Sigma^{(j)}(x)$ of two-scale fields $u^{(j)}(x, y)$ and
 613 $s^{(j)}(x, y)$ are defined for $j \geq 0$,

$$614 \quad \mathcal{U}^{(j)}(x) = \langle u^{(j)} \rangle \quad \text{and} \quad \Sigma^{(j)}(x) = \langle s^{(j)} \rangle. \tag{A.2}$$

615 The local Ω -periodicity of stress fields $s^{(j)}(x, y)$ over the variable y implies
 616 the following relation, that is useful when Eqs. (A.1b), (A.1d), (A.1f) and
 617 (A.1h) is y -averaged

$$618 \quad \langle \partial_y s^{(j)} \rangle = 0. \tag{A.3}$$

619 Equation (A.1a) shows that $u^{(0)}(x, y)$ is independent of y . It is therefore
 620 purely macroscopic, and reads

$$621 \quad u^{(0)}(x, y) \equiv \mathcal{U}^{(0)}(x). \tag{A.4}$$

Equations (A.1b) and (A.1c) show that $u^{(1)}(x, y)$ and $s^{(0)}(x, y)$ are forced at the macroscopic scale by $\partial_x \mathcal{U}^{(0)}$. Thus they write

$$u^{(1)}(x, y) = \mathcal{U}^{(1)}(x) + \chi_1^{(1)}(y) \partial_x^1 \mathcal{U}^{(0)}, \quad (\text{A.5a})$$

$$s^{(0)}(x, y) = q_0^{(0)}(y) \partial_x^1 \mathcal{U}^{(0)}, \quad (\text{A.5b})$$

where cell field $\chi_1^{(1)}(y)$ and local modulus $q_0^{(0)}(y)$ are Ω -periodic and satisfy the cell problem

$$\partial_y q_0^{(0)} = 0, \quad (\text{A.6a})$$

$$q_0^{(0)} = a(1 + \partial_y \chi_1^{(1)}), \quad (\text{A.6b})$$

with the condition $\langle \chi_1^{(1)} \rangle = 0$ so that $\mathcal{U}^{(1)} = \langle u^{(1)} \rangle$. Then, the equations governing the macroscopic field $\mathcal{U}^{(0)}$ are obtained by y -averaging (A.5b) and (A.1d),

$$\Sigma^{(0)} = E_0 \partial_x^1 \mathcal{U}^{(0)}, \quad (\text{A.7a})$$

$$\partial_x \Sigma^{(0)} = \rho_0 (\partial_t^2 \mathcal{U}^{(0)} - f(x)), \quad (\text{A.7b})$$

622 where effective material parameters are given by

$$623 \quad E_0 = \langle q_0^{(0)} \rangle = \langle a(1 + \partial_y \chi_1^{(1)})^2 \rangle, \quad \rho_0 = \langle \rho \rangle. \quad (\text{A.8})$$

624 Hence, both E_0 and ρ_0 are positive. The second expression for E_0 in Eq. (A.8)
625 follows from the weak formulation of cell problem (A.6) with $\chi_1^{(1)}$ as the test-
626 field [17]

$$627 \quad \langle \chi_1^{(1)} \partial_y q_0^{(0)} \rangle = - \langle (\partial_y \chi_1^{(1)}) a(1 + \partial_y \chi_1^{(1)}) \rangle = 0. \quad (\text{A.9})$$

628 Combination of (A.7a) and (A.7b) yields the equation for the leading-order
629 displacement $\mathcal{U}^{(0)}$

$$630 \quad \mathcal{C}_0(\mathcal{U}^{(0)}) \stackrel{\text{def}}{=} \rho_0 \partial_t^2 \mathcal{U}^{(0)} - E_0 \partial_x^2 \mathcal{U}^{(0)} = \rho_0 f(x), \quad (\text{A.10})$$

631 which corresponds to elastodynamics in Cauchy media, with the density ρ_0
632 and elasticity modulus E_0 . From (A.6a), it follows that $q_0^{(0)}$ is uniform and
633 hence equal to its mean value E_0 . Then, averaging $q_0^{(0)}/a$ from (A.6b) with
634 $\langle \partial_y \chi_1^{(1)} \rangle = 0$ due to Ω -periodicity leads to the relation for the elastic modulus

$$635 \quad q_0^{(0)} \equiv E_0 = \left\langle \frac{1}{a(y)} \right\rangle^{-1}. \quad (\text{A.11})$$

Expressions for $\partial_t^2 \mathcal{U}^{(0)} - f(x)$ given in (A.7a) and $u^{(1)}$ in (A.5a) are substituted
into (A.1d) and (A.1e) to yield:

$$\partial_y s^{(1)} = r_0^{(0)}(y) \partial_x^2 \mathcal{U}^{(0)}, \quad (\text{A.12a})$$

$$s^{(1)} = a(\partial_y u^{(2)} + \partial_x \mathcal{U}^{(1)} + \chi_1^{(1)}(y) \partial_x^2 \mathcal{U}^{(0)}). \quad (\text{A.12b})$$

637 Due to (A.5b) and (A.7a), the source term $r_0^{(0)}$ in (A.12a) writes

$$638 \quad r_0^{(0)}(y) = \frac{\rho(y)}{\rho_0^{(0)}} E_0^{(0)} - q_0^{(0)}(y) = \left(\frac{\rho(y)}{\rho_0^{(0)}} - 1 \right) E_0^{(0)}. \quad (\text{A.13})$$

Equations (A.12a) to (A.13) show that $u^{(2)}$ and $s^{(1)}$ are forced by both $\partial_x \mathcal{U}^{(1)}$
and $\partial_x^2 \mathcal{U}^{(0)}$ according to

$$u^{(2)}(x, y) = \mathcal{U}^{(2)}(x) + \chi_1^{(1)} \partial_x^1 \mathcal{U}^{(1)} + \chi_2^{(2)} \partial_x^2 \mathcal{U}^{(0)}, \quad (\text{A.14a})$$

$$s^{(1)}(x, y) = q_0^{(0)} \partial_x^1 \mathcal{U}^{(1)} + q_1^{(1)} \partial_x^2 \mathcal{U}^{(0)}. \quad (\text{A.14b})$$

The cell field $\chi_2^{(2)}(y)$ and local modulus $q_1^{(1)}(y)$ are Ω -periodic and satisfy the
cell problem

$$\partial_y q_1^{(1)} = r_0^{(0)}(y) \quad (\text{A.15a})$$

$$q_1^{(1)} = a \left(\chi_1^{(1)}(y) + \partial_y \chi_2^{(2)} \right), \quad (\text{A.15b})$$

639 with $\langle \chi_2^{(2)} \rangle = 0$, so that $\mathcal{U}^{(2)} = \langle u^{(2)} \rangle$. Averaging $q_1^{(1)}/a$ from (A.15b) with
 640 $\langle \partial_y \chi_2^{(2)} \rangle = 0$ due to Ω -periodicity leads to

$$641 \quad \left\langle \frac{q_1^{(1)}(y)}{a(y)} \right\rangle = \left\langle \chi_1^{(1)}(y) + \partial_y \chi_2^{(2)} \right\rangle \equiv 0. \quad (\text{A.16})$$

Then, the equations governing the macroscopic field $\mathcal{U}^{(1)}$ are obtained by
 y -averaging (A.14b) and (A.1f),

$$\Sigma^{(1)} = E_0^{(0)} \partial_x^1 \mathcal{U}^{(1)} + E_1^{(1)} \partial_x^2 \mathcal{U}^{(0)}, \quad (\text{A.17a})$$

$$\partial_x \Sigma^{(1)} = \rho_0^{(0)} \partial_t^2 \mathcal{U}^{(1)} + \rho_1^{(1)} \partial_t^2 \partial_x \mathcal{U}^{(0)}, \quad (\text{A.17b})$$

642 where effective material parameters are given by

$$643 \quad E_1^{(1)} = \left\langle q_1^{(1)} \right\rangle, \quad \rho_1^{(1)} = \left\langle \rho \chi_1^{(1)} \right\rangle. \quad (\text{A.18})$$

644 The weak formulation of cell problems (A.6) and (A.15) with $\chi_1^{(1)}$ and $\chi_2^{(2)}$
 645 as test-fields yields [20]

$$646 \quad \begin{aligned} E_1^{(1)} &= \left\langle \chi_1^{(1)} \partial_y q_1^{(1)} - \chi_2^{(2)} \partial_y q_0^{(0)} + \chi_1^{(1)} q_0^{(0)} \right\rangle \\ &= \left\langle \chi_1^{(1)} r_0^{(0)} + \chi_1^{(1)} q_0^{(0)} \right\rangle = \rho_1^{(1)} E_0 / \rho_0. \end{aligned} \quad (\text{A.19})$$

647 Combination of (A.17a) and (A.17b) leads to

$$648 \quad \mathcal{C}_0(\mathcal{U}^{(1)}) = -\partial_x \{ \rho_1^{(1)} \partial_t^2 \mathcal{U}^{(0)} - E_1^{(1)} \partial_x^2 \mathcal{U}^{(0)} \}. \quad (\text{A.20})$$

649 Multiplication of (A.10) by $\rho_1^{(1)}/\rho_0$ and use of (A.19) gives

$$650 \quad \rho_1^{(1)} \partial_t^2 \mathcal{U}^{(0)} - E_1^{(1)} \partial_x^2 \mathcal{U}^{(0)} = \rho_1^{(1)} f(x), \quad (\text{A.21})$$

651 which is analogous to classical elastodynamics in Cauchy media, with $\rho_1^{(1)}$ and
 652 $E_1^{(1)}$ as density and elasticity modulus. Substitution of (A.21) into (A.20)
 653 provides

$$654 \quad \mathcal{C}_0(\mathcal{U}^{(1)}) = -\rho_0 h^{(1)} \partial_x f(x), \quad h^{(1)} = \rho_1^{(1)} / \rho_0, \quad (\text{A.22})$$

655 which shows that $\mathcal{U}^{(1)}$ is actually forced by the gradient of the bulk force,
 656 $\partial_x f(x)$. As previously, (A.22) is multiplied by $\rho_1^{(1)}/\rho_0$ and combined with
 657 (A.19) to give

$$658 \quad \rho_1^{(1)} \partial_t^2 \mathcal{U}^{(1)} - E_1^{(1)} \partial_x^2 \mathcal{U}^{(1)} = -\rho_0 (h^{(1)})^2 \partial_x f(x). \quad (\text{A.23})$$

659 Substitution of (A.5a) and (A.14b) into (A.1f), while using (A.17a) and
 660 (A.17b) to express $\partial_t^2 \mathcal{U}^{(1)}$ and $\Sigma^{(1)}$ provides

$$661 \quad \partial_y s^{(2)} = r_0^{(0)} \partial_x^2 \mathcal{U}^{(1)} + r_1^{(1)} \partial_x^3 \mathcal{U}^{(0)} + \rho_0 \tilde{r}_1^{(1)} \partial_t^2 \partial_x \mathcal{U}^{(0)}, \quad (\text{A.24})$$

where the source terms $r_1^{(1)}(y)$ and $\tilde{r}_1^{(1)}(y)$ read

$$r_1^{(1)}(y) = \frac{\rho(y)}{\rho_0} E_1^{(1)} - q_1^{(1)}(y), \quad (\text{A.25a})$$

$$\tilde{r}_1^{(1)}(y) = \frac{\rho(y)}{\rho_0} \left(\chi_1^{(1)}(y) - \frac{\rho_1^{(1)}}{\rho_0} \right). \quad (\text{A.25b})$$

662 Further, substitution of (A.14a) into (A.1g) yields

$$663 \quad s^{(2)} = a(\partial_y u^{(3)} + \partial_x \mathcal{U}^{(2)} + \chi_1^{(1)} \partial_x^2 \mathcal{U}^{(1)} + \chi_2^{(2)} \partial_x^3 \mathcal{U}^{(0)}). \quad (\text{A.26})$$

Equations (A.24) and (A.26) evidence that $u^{(3)}(x, y)$ and $s^{(2)}(x, y)$ are forced
 at the macroscopic scale by $\partial_x \mathcal{U}^{(2)}$, $\partial_x^2 \mathcal{U}^{(1)}$, $\partial_x^3 \mathcal{U}^{(0)}$, and $\partial_t^2 \partial_x \mathcal{U}^{(0)}$ according to

$$u^{(3)}(x, y) = \mathcal{U}^{(3)} + \chi_1^{(1)} \partial_x \mathcal{U}^{(2)} + \chi_2^{(2)} \partial_x^2 \mathcal{U}^{(1)} + \chi_3^{(3)} \partial_x^3 \mathcal{U}^{(0)} + \rho_0 \psi^{(3)} \partial_t^2 \partial_x \mathcal{U}^{(0)}, \quad (\text{A.27a})$$

$$s^{(2)}(x, y) = q_0^{(0)} \partial_x \mathcal{U}^{(2)} + q_1^{(1)} \partial_x^2 \mathcal{U}^{(1)} + q_2^{(2)} \partial_x^3 \mathcal{U}^{(0)} + \rho_0 p^{(2)} \partial_t^2 \partial_x \mathcal{U}^{(0)}. \quad (\text{A.27b})$$

The cell fields $\chi_3^{(3)}(y)$ and $\psi^{(3)}(y)$, and associated local moduli $q_2^{(2)}(y)$ and $p^{(2)}(y)$ are Ω -periodic and satisfy the cell problems

$$\partial_y q_2^{(2)} = r_1^{(1)}, \quad q_2^{(2)} = a \left(\chi_2^{(2)}(y) + \partial_y \chi_3^{(3)} \right), \quad (\text{A.28a})$$

$$\partial_y p^{(2)} = \tilde{r}_1^{(1)}, \quad p^{(2)} = a \partial_y \psi^{(3)}, \quad (\text{A.28b})$$

664 with the condition $\langle \chi_3^{(3)} \rangle = 0$ and $\langle \psi^{(3)} \rangle = 0$, so that $\mathcal{U}^{(3)} = \langle u^{(3)} \rangle$. Averaging
 665 $q_2^{(2)}/a$ and $p^{(2)}/a$ with $\langle \partial_y \chi_3^{(3)} \rangle = 0$ and $\langle \partial_y \psi^{(3)} \rangle = 0$ due to Ω -periodicity
 666 yields

$$667 \quad \left\langle \frac{q_2^{(2)}(y)}{a(y)} \right\rangle = 0 \quad \text{and} \quad \left\langle \frac{p^{(2)}(y)}{a(y)} \right\rangle = 0. \quad (\text{A.29})$$

668 In (A.27b), we choose to involve the derivative $\partial_t^2 \partial_x \mathcal{U}^{(0)}$ in the stress field.
 669 Using the wave equation (A.10) at dominant order, this derivative is trans-
 670 formed into $\rho_0 \partial_t^2 \partial_x \mathcal{U}^{(0)} = E_0 \partial_x^3 \mathcal{U}^{(0)} + \rho_0 \partial_x f$. In the absence of bulk force
 671 $f = 0$, this procedure is usually applied, so as to keep only high-order space
 672 derivatives $\partial_x^3 \mathcal{U}^{(0)}$ in the expression of the stress field [20, 13, 11, 14]. With
 673 bulk force, we prefer to keep the space-time derivative $\rho_0 \partial_t^2 \partial_x \mathcal{U}^{(0)}$ in the ef-
 674 fective constitutive relation (A.27b) rather than involving the bulk force in
 675 it. This choice leads to define the cell problems according to (A.28).

Finally, the equations governing the macroscopic field $\mathcal{U}^{(2)}$ are obtained by y -averaging (A.27b) and (A.1h),

$$\begin{aligned} \Sigma^{(2)} &= E_0 \partial_x \mathcal{U}^{(2)} + E_1^{(1)} \partial_x^2 \mathcal{U}^{(1)} \\ &\quad + E_2^{(2)} \partial_x^3 \mathcal{U}^{(0)} + \rho_0 J_1^{(2)} \partial_t^2 \partial_x \mathcal{U}^{(0)}, \end{aligned} \quad (\text{A.30a})$$

$$\begin{aligned} \partial_x \Sigma^{(2)} &= \rho_0 \partial_t^2 \mathcal{U}^{(2)} + \rho_1^{(1)} \partial_x \partial_t^2 \mathcal{U}^{(1)} \\ &\quad + \rho_2^{(2)} \partial_x^2 \partial_t^2 \mathcal{U}^{(0)}, \end{aligned} \quad (\text{A.30b})$$

676 with effective material parameters given by

$$677 \quad E_2^{(2)} = \langle q_2^{(2)} \rangle, \quad J_1^{(2)} = \langle p^{(2)} \rangle, \quad \rho_2^{(2)} = \langle \rho \chi_2^{(2)} \rangle. \quad (\text{A.31})$$

678 Weak formulation of cell problems (A.28b) and (A.15) with $\chi_1^{(1)}$ and $\psi^{(3)}$ as
679 test-fields yields

$$680 \quad \begin{aligned} J_1^{(2)} &= \langle \chi_1^{(1)} \partial_y p^{(2)} - \psi^{(3)} \partial_y q_0^{(0)} \rangle \\ &= \left\langle \frac{\rho}{\rho_0} (\chi_1^{(1)})^2 \right\rangle - \left\langle \frac{\rho}{\rho_0} \chi_1^{(1)} \right\rangle^2 > 0. \end{aligned} \quad (\text{A.32})$$

681 Combination of (A.30a) and (A.30b) with (A.23) yields the equation for the
682 displacement $\mathcal{U}^{(2)}$

$$683 \quad \begin{aligned} \mathcal{C}_0(\mathcal{U}^{(2)}) &= \rho_0 (h^{(1)})^2 \partial_x^2 f(x) \\ &- \left\{ -\rho_0 \Gamma_t^{(2)} \partial_x^2 \partial_t^2 \mathcal{U}^{(0)} - E_0 \Gamma_x^{(2)} \partial_x^4 \mathcal{U}^{(0)} \right\}. \end{aligned} \quad (\text{A.33})$$

684 where characteristic surfaces $\Gamma_t^{(2)}$ and $\Gamma_x^{(2)}$ are defined by

$$685 \quad \rho_0 \Gamma_t^{(2)} = \rho_0 J_1^{(2)} - \rho_2^{(2)}, \quad E_0 \Gamma_x^{(2)} = E_2^{(2)}. \quad (\text{A.34})$$

From (A.10) and for any α_t and α_x , one gets

$$(1 + \alpha_t - \alpha_t) \partial_x^2 \partial_t^2 \mathcal{U}^{(0)} = \frac{\rho_0}{E_0} (\partial_t^4 \mathcal{U}^{(0)} - \partial_t^2 f), \quad (\text{A.35a})$$

$$(1 + \alpha_x - \alpha_x) \partial_x^4 \mathcal{U}^{(0)} = \frac{\rho_0}{E_0} (\partial_x^2 \partial_t^2 \mathcal{U}^{(0)} - \partial_x^2 f). \quad (\text{A.35b})$$

It results into

$$\partial_x^2 \partial_t^2 \mathcal{U}^{(0)} = (1 + \alpha_t) \partial_x^2 \partial_t^2 \mathcal{U}^{(0)} - \alpha_t \frac{\rho_0}{E_0} (\partial_t^4 \mathcal{U}^{(0)} - \partial_t^2 f), \quad (\text{A.36a})$$

$$\partial_x^4 \mathcal{U}^{(0)} = (1 + \alpha_x) \frac{\rho_0}{E_0} (\partial_x^2 \partial_t^2 \mathcal{U}^{(0)} - \partial_x^2 f) - \alpha_x \partial_x^4 \mathcal{U}^{(0)}, \quad (\text{A.36b})$$

686 which, once substituted into (A.33) leads to (61).

687 **Appendix B. Cell functions and effective properties in periodic**
688 **multilaminate materials**

689 Here, cell functions and effective material parameters defined through
690 two-scale asymptotic homogenization in [Appendix A](#) are given for the peri-
691 odic multilaminate material. It consists of the ℓ -sized unit cell Ω made of the
692 $n = 1 \dots \mathcal{N}$ homogeneous elastic layers $\Omega^{[n]} = [L^{[n]}, L^{[n+1]})$ having the densi-
693 ties $\rho^{[n]}$, local elastic moduli $a^{[n]}$, and thickness $\ell^{[n]} = \phi^{[n]}\ell = L^{[n+1]} - L^{[n]}$,
694 with filling fractions $\phi^{[n]}$ and boundaries at abscissa $L^{[n]}$ so that

$$695 \quad \sum_{n=1}^{\mathcal{N}} \phi^{[n]} = 1, \quad L^{[n]} = \sum_{m=1}^{n-1} \ell^{[m]} = \left(\sum_{m=1}^{n-1} \phi^{[m]} \right) \ell, \quad (\text{B.1})$$

696 with $L^{[1]} = 0$ and $L^{[\mathcal{N}+1]} = \ell$. Here and in what follows, the usual convention
697 that the sum \sum_a^b is zero if $b < a$ is adopted. Further, space, fields and
698 parameters have been re-scaled to physical scale, with $x = \epsilon y$ and $q_j = \epsilon^j q_j^{(j)}$
699 for instance. The local normalised coordinate $\xi^{[n]}$ holding on layer $\Omega^{[n]}$ is also
700 defined as follows, for $n \geq 1$,

$$701 \quad \forall x \in [L^{[n]}, L^{[n+1]}], \quad \xi^{[n]} = \frac{x - L^{[n]}}{\ell} \in [0, \phi^{[n]}]. \quad (\text{B.2})$$

702 Explicit resolution of the cell problems is provided in the general case of the
703 multilaminate materials; then, formula are provided in the simple case of the
704 bilaminate materials with $\mathcal{N} = 2$.

705 *Appendix B.1. General formulation*

706 First, equations [\(A.8\)](#) and [\(A.11\)](#) provide

$$707 \quad \rho_0 = \sum_{n=1}^{\mathcal{N}} \phi^{[n]} \rho^{[n]}, \quad q_0 \equiv E_0 = \left(\sum_{n=1}^{\mathcal{N}} \frac{\phi^{[n]}}{a^{[n]}} \right)^{-1}. \quad (\text{B.3})$$

Then, successive integrations of Eqs. (A.6b) and (A.15a) to solve for χ_1 and q_1 , yield the cell functions in the following form of linear functions on layer $\Omega^{[n]}$,

$$\frac{\chi_1(\xi^{[n]})}{\ell} = \vartheta_E^{[n]} \xi^{[n]} + \mathcal{X}_1^{[n]} - \tilde{\chi}_1, \quad (\text{B.4a})$$

$$\frac{q_1(\xi^{[n]})}{E_0 \ell} = \vartheta_\rho^{[n]} \xi^{[n]} + Q_1^{[n]} - \tilde{q}_1. \quad (\text{B.4b})$$

708 Here, the dimensionless factors $\vartheta_E^{[n]}$ and $\vartheta_\rho^{[n]}$ read

$$709 \quad \vartheta_E^{[n]} = \frac{E_0}{a^{[n]}} - 1 \quad \text{and} \quad \vartheta_\rho^{[n]} = \frac{\rho^{[n]}}{\rho_0} - 1, \quad (\text{B.5})$$

710 while factors $\mathcal{X}_1^{[n]}$ and $Q_1^{[n]}$ are defined to ensure continuity and periodicity
711 of the cell functions,

$$712 \quad \mathcal{X}_1^{[n]} = \sum_{m=1}^{n-1} \vartheta_E^{[m]} \phi^{[m]}, \quad Q_1^{[n]} = \sum_{m=1}^{n-1} \vartheta_\rho^{[m]} \phi^{[m]}, \quad (\text{B.6})$$

and dimensionless parameters $\tilde{\chi}_1$ and \tilde{q}_1 are prescribed by conditions of zero mean values $\langle \chi_1 \rangle = 0$ and $\langle q_1/a \rangle = 0$,

$$\tilde{\chi}_1 = \sum_{n=1}^{\mathcal{N}} \left[\vartheta_E^{[n]} \frac{(\phi^{[n]})^2}{2} + \mathcal{X}_1^{[n]} \phi^{[n]} \right], \quad (\text{B.7a})$$

$$\tilde{q}_1 = \sum_{n=1}^{\mathcal{N}} \frac{E_0}{a^{[n]}} \left[\vartheta_\rho^{[n]} \frac{(\phi^{[n]})^2}{2} + Q_1^{[n]} \phi^{[n]} \right]. \quad (\text{B.7b})$$

For efficient calculations of $\mathcal{X}_1^{[n]}$ and $Q_1^{[n]}$, it is worth noting the following recurrence relations for $n \geq 1$,

$$\mathcal{X}_1^{[n+1]} = \mathcal{X}_1^{[n]} + \vartheta_E^{[n]} \phi^{[n]}, \quad (\text{B.8a})$$

$$Q_1^{[n+1]} = Q_1^{[n]} + \vartheta_\rho^{[n]} \phi^{[n]}, \quad (\text{B.8b})$$

and following relations due to ℓ -periodicity,

$$\mathcal{X}_1^{[\mathcal{N}+1]} = \sum_{m=1}^{\mathcal{N}} \vartheta_E^{[m]} \phi^{[m]} = 0 = \mathcal{X}_1^{[1]}, \quad (\text{B.9a})$$

$$Q_1^{[\mathcal{N}+1]} = \sum_{m=1}^{\mathcal{N}} \vartheta_\rho^{[m]} \phi^{[m]} = 0 = Q_1^{[1]}. \quad (\text{B.9b})$$

As a result of cell functions in Eq. (B.4), the material parameters ρ_1 and E_1 defined in Eq. (A.18) are given by

$$\frac{\rho_1}{\rho_0 \ell} = \sum_{n=1}^{\mathcal{N}} \vartheta_\rho^{[n]} \left[\vartheta_E^{[n]} \frac{(\phi^{[n]})^2}{2} + \mathcal{X}_1^{[n]} \phi^{[n]} \right], \quad (\text{B.10a})$$

$$\frac{E_1}{E_0 \ell} = - \sum_{n=1}^{\mathcal{N}} \vartheta_E^{[n]} \left[\vartheta_\rho^{[n]} \frac{(\phi^{[n]})^2}{2} + Q_1^{[n]} \phi^{[n]} \right]. \quad (\text{B.10b})$$

At order ϵ^2 , successive integrations of (A.15b), (A.28a) and (A.28b) to solve for χ_2 , q_2 , and p yield the cell functions in the form of second-order polynomials on layer $\Omega^{[n]}$,

$$\frac{\chi_2(\xi^{[n]})}{\ell^2} = \vartheta_d^{[n]} \frac{(\xi^{[n]})^2}{2} + \mathcal{Z}^{[n]} \xi^{[n]} + \mathcal{X}_2^{[n]} - \tilde{\chi}_2 \quad (\text{B.11a})$$

$$\frac{q_2(\xi^{[n]})}{E_0 \ell^2} = -\vartheta_\rho^{[n]} \frac{(\xi^{[n]})^2}{2} + \mathcal{Y}^{[n]} \xi^{[n]} + Q_2^{[n]} - \tilde{q}_2, \quad (\text{B.11b})$$

$$\frac{p(\xi^{[n]})}{\ell^2} = \frac{\rho^{[n]}}{\rho_0} \vartheta_E^{[n]} \frac{(\xi^{[n]})^2}{2} + \mathcal{R}^{[n]} \xi^{[n]} + P^{[n]} - \tilde{p}. \quad (\text{B.11c})$$

Here, dimensionless coefficients read

$$\vartheta_d^{[n]} = \frac{E_0}{a^{[n]}} \vartheta_\rho^{[n]} - \vartheta_E^{[n]}, \quad (\text{B.12a})$$

$$\mathcal{Z}^{[n]} = \frac{E_0}{a^{[n]}} \left(Q_1^{[n]} - \tilde{q}_1 \right) - \left(\mathcal{X}_1^{[n]} - \tilde{\chi}_1 \right), \quad (\text{B.12b})$$

$$\mathcal{Y}^{[n]} = \frac{\rho^{[n]}}{\rho_0} \frac{E_1}{E_0 \ell} - \left(Q_1^{[n]} - \tilde{q}_1 \right), \quad (\text{B.12c})$$

$$\mathcal{R}^{[n]} = \frac{\rho^{[n]}}{\rho_0} \left(\mathcal{X}_1^{[n]} - \tilde{\chi}_1 - \frac{\rho_1}{\rho_0 \ell} \right), \quad (\text{B.12d})$$

while factors $\mathcal{X}_2^{[n]}$, $Q_2^{[n]}$ and $P^{[n]}$ are defined to ensure continuity and periodicity of the cell functions,

$$\mathcal{X}_2^{[n]} = \sum_{m=1}^{n-1} \vartheta_d^{[m]} \frac{(\phi^{[m]})^2}{2} + \mathcal{Z}^{[m]} \phi^{[m]}, \quad (\text{B.13a})$$

$$Q_2^{[n]} = \sum_{m=1}^{n-1} -\vartheta_\rho^{[m]} \frac{(\phi^{[m]})^2}{2} + \mathcal{Y}^{[m]} \phi^{[m]}, \quad (\text{B.13b})$$

$$P^{[n]} = \sum_{m=1}^{n-1} \frac{\rho^{[m]}}{\rho_0} \vartheta_E^{[m]} \frac{(\phi^{[m]})^2}{2} + \mathcal{R}^{[m]} \phi^{[m]}, \quad (\text{B.13c})$$

and parameters $\tilde{\chi}_2$, \tilde{q}_2 and \tilde{p} are prescribed by conditions of zero mean values $\langle \chi_2 \rangle = 0$, $\langle q_2/a \rangle = 0$ and $\langle p/a \rangle = 0$,

$$\tilde{\chi}_2 = \sum_{n=1}^{\mathcal{N}} \vartheta_d^{[n]} \frac{(\phi^{[n]})^3}{6} + \mathcal{Z}^{[n]} \frac{(\phi^{[n]})^2}{2} + \mathcal{X}_2^{[n]} \phi^{[n]}, \quad (\text{B.14a})$$

$$\tilde{q}_2 = \sum_{n=1}^{\mathcal{N}} \frac{E_0}{a^{[n]}} \left[-\vartheta_\rho^{[n]} \frac{(\phi^{[n]})^3}{6} + \mathcal{Y}^{[n]} \frac{(\phi^{[n]})^2}{2} + Q_2^{[n]} \phi^{[n]} \right], \quad (\text{B.14b})$$

$$\tilde{p} = \sum_{n=1}^{\mathcal{N}} \frac{E_0}{a^{[n]}} \left[\frac{\rho^{[n]}}{\rho_0} \vartheta_E^{[n]} \frac{(\phi^{[n]})^3}{6} + \mathcal{R}^{[n]} \frac{(\phi^{[n]})^2}{2} + P^{[n]} \phi^{[n]} \right]. \quad (\text{B.14c})$$

For efficient calculations of $\mathcal{X}_2^{[n]}$, $Q_2^{[n]}$ and $P^{[n]}$, one notices

$$\mathcal{X}_2^{[n+1]} = \mathcal{X}_2^{[n]} + \vartheta_d^{[n]} \frac{(\phi^{[n]})^2}{2} + \mathcal{Z}^{[n]} \phi^{[n]}, \quad (\text{B.15a})$$

$$Q_2^{[n+1]} = Q_2^{[n]} - \vartheta_\rho^{[n]} \frac{(\phi^{[n]})^2}{2} + \mathcal{Y}^{[n]} \phi^{[n]}, \quad (\text{B.15b})$$

$$P^{[n+1]} = P^{[n]} + \frac{\rho^{[n]}}{\rho_0} \vartheta_E^{[n]} \frac{(\phi^{[n]})^2}{2} + \mathcal{R}^{[n]} \phi^{[n]}, \quad (\text{B.15c})$$

and following relations due to ℓ -periodicity,

$$\mathcal{X}_2^{[N+1]} = \sum_{m=1}^{\mathcal{N}} \vartheta_d^{[m]} \frac{(\phi^{[m]})^2}{2} + \mathcal{Z}^{[m]} \phi^{[m]} = 0 = \mathcal{X}_2^{[1]}, \quad (\text{B.16a})$$

$$Q_2^{[N+1]} = \sum_{m=1}^{\mathcal{N}} -\vartheta_\rho^{[m]} \frac{(\phi^{[m]})^2}{2} + \mathcal{Y}^{[m]} \phi^{[m]} = 0 = Q_2^{[1]}. \quad (\text{B.16b})$$

$$P^{[N+1]} = \sum_{m=1}^{\mathcal{N}} \frac{\rho^{[m]}}{\rho_0} \vartheta_E^{[m]} \frac{(\phi^{[m]})^2}{2} + \mathcal{R}^{[m]} \phi^{[m]} = 0 = P^{[1]}. \quad (\text{B.16c})$$

From (B.11), the parameters ρ_2 , E_2 and J_1 in (A.31) read

$$\frac{\rho_2}{\rho_0 \ell^2} = \sum_{n=1}^{\mathcal{N}} \vartheta_\rho^{[n]} \left[\vartheta_d^{[n]} \frac{(\phi^{[n]})^3}{6} + \mathcal{Z}^{[n]} \frac{(\phi^{[n]})^2}{2} + \mathcal{X}_2^{[n]} \phi^{[n]} \right], \quad (\text{B.17a})$$

$$\frac{E_2}{E_0 \ell^2} = - \sum_{n=1}^{\mathcal{N}} \vartheta_E^{[n]} \left[-\vartheta_\rho^{[n]} \frac{(\phi^{[n]})^3}{6} + \mathcal{Y}^{[n]} \frac{(\phi^{[n]})^2}{2} + Q_2^{[n]} \phi^{[n]} \right], \quad (\text{B.17b})$$

$$\frac{J_1}{\ell^2} = - \sum_{n=1}^{\mathcal{N}} \vartheta_E^{[n]} \left[\frac{\rho^{[n]}}{\rho_0} \vartheta_E^{[n]} \frac{(\phi^{[n]})^3}{6} + \mathcal{R}^{[n]} \frac{(\phi^{[n]})^2}{2} + P^{[n]} \phi^{[n]} \right]. \quad (\text{B.17c})$$

713 while Γ_x , Γ_t and B are calculated according to

$$714 \quad \frac{\Gamma_x}{\ell^2} = \frac{E_2}{E_0 \ell^2}, \quad \frac{\Gamma_t}{\ell^2} = \frac{J_1}{\ell^2} - \frac{\rho_2}{\rho_0 \ell^2}, \quad \frac{B}{\ell^2} = \frac{\Gamma_x + \Gamma_t}{\ell^2}. \quad (\text{B.18})$$

715 *Appendix B.2. Case of the bilaminate materials*

In the case of the periodic bilaminate material ($\mathcal{N} = 2$), cell functions result in the following effective material parameters,

$$\rho_0 = \phi^{[1]}\rho^{[1]} + \phi^{[2]}\rho^{[2]}, \quad \frac{1}{E_0} = \frac{\phi^{[1]}}{a_{[1]}} + \frac{\phi^{[2]}}{a_{[2]}}, \quad (\text{B.19a})$$

$$\rho_1 = 0, \quad E_1 = \rho_1 E_0 / \rho_0 = 0, \quad (\text{B.19b})$$

$$\frac{\rho_2}{\rho_0} = -\frac{\ell^2}{12} \left(\vartheta_\rho^{[1]}\vartheta_d^{[1]}(\phi^{[1]})^3 + \vartheta_\rho^{[2]}\vartheta_d^{[2]}(\phi^{[2]})^3 \right), \quad (\text{B.19c})$$

$$\frac{E_2}{E_0} = -\frac{\ell^2}{12} \left(\vartheta_\rho^{[1]}\vartheta_E^{[1]}(\phi^{[1]})^3 + \vartheta_\rho^{[2]}\vartheta_E^{[2]}(\phi^{[2]})^3 \right), \quad (\text{B.19d})$$

$$J_1 = \frac{\ell^2}{12} \left(\frac{\rho^{[1]}}{\rho_0} (\vartheta_E^{[1]})^2 (\phi^{[1]})^3 + \frac{\rho^{[2]}}{\rho_0} (\vartheta_E^{[2]})^2 (\phi^{[2]})^3 \right), \quad (\text{B.19e})$$

$$J_2 = \frac{\ell^2}{12} \left(\frac{E_0}{a_{[1]}} (\vartheta_\rho^{[1]})^2 (\phi^{[1]})^3 + \frac{E_0}{a_{[2]}} (\vartheta_\rho^{[2]})^2 (\phi^{[2]})^3 \right), \quad (\text{B.19f})$$

716 where $J_2 = -(\rho_2/\rho_0 + E_2/E_0)$. Relations in (B.19) show the symmetric role
717 of layers $\Omega^{[1]}$ and $\Omega^{[2]}$. Using (B.9) and

$$718 \quad (\phi^{[1]})^2 \vartheta_\rho^{[1]}\vartheta_E^{[1]} = (\phi^{[2]})^2 \vartheta_\rho^{[2]}\vartheta_E^{[2]}, \quad (\text{B.20})$$

the following relations are found,

$$J_1 = \frac{(\ell^{[1]})^2}{12} (\vartheta_E^{[1]})^2 = \frac{(\ell^{[2]})^2}{12} (\vartheta_E^{[2]})^2 \geq 0, \quad (\text{B.21a})$$

$$J_2 = \frac{(\ell^{[1]})^2}{12} (\vartheta_\rho^{[1]})^2 = \frac{(\ell^{[2]})^2}{12} (\vartheta_\rho^{[2]})^2 \geq 0, \quad (\text{B.21b})$$

$$\frac{E_2}{E_0} = -\frac{(\ell^{[1]})^2}{12} \vartheta_\rho^{[1]}\vartheta_E^{[1]} = -\frac{(\ell^{[2]})^2}{12} \vartheta_\rho^{[2]}\vartheta_E^{[2]}. \quad (\text{B.21c})$$

719 The characteristic surface $B = \Gamma_x + \Gamma_t = J_1 + J_2 + 2E_2/E_0$ reads

$$720 \quad B = \frac{(\ell^{[1]})^2}{12} (\vartheta_\rho^{[1]} - \vartheta_E^{[1]})^2 = \frac{(\ell^{[2]})^2}{12} (\vartheta_\rho^{[2]} - \vartheta_E^{[2]})^2. \quad (\text{B.22})$$

721 **Appendix C. Plane Wave Method for dispersion relation in peri-**
722 **odic laminates**

723 The dispersion relation in 1-D periodic multi-laminate materials can be
724 computed according to the Plane Wave Method. A medium with ℓ -sized
725 unit cell Ω made of $n = 1 \dots \mathcal{N}$ homogeneous elastic layers $\Omega^{[n]} = [x^{[n]}, x^{[n+1]}]$
726 of thickness $\ell^{[n]} = x^{[n+1]} - x^{[n]} = \phi^{[n]}\ell$, densities $\rho^{[n]}$, local elastic moduli
727 $a^{[n]}$, and wave speed $c^{[n]} = \sqrt{a^{[n]}/\rho^{[n]}}$ is considered. In the layer $\Omega^{[n]}$, the
728 displacement $u^{[n]}(x) e^{-i\omega t}$ writes

$$729 \quad u^{[n]}(x) = \mathbb{U}_1^{[n]} e^{ik^{[n]}(x-x^{[n]})} + \mathbb{U}_2^{[n]} e^{-ik^{[n]}(x-x^{[n]})}, \quad (\text{C.1})$$

730 where $\mathbb{U}_1^{[n]}$ and $\mathbb{U}_2^{[n]}$ are complex amplitudes and $k^{[n]} = \omega/c^{[n]}$ is the wavenum-
731 ber in the layer $\Omega^{[n]}$. Continuity on the displacement $u^{[n]} = u^{[n+1]}$, and stress
732 $a^{[n]}\partial_x u^{[n]} = a^{[n+1]}\partial_x u^{[n+1]}$ at point $x^{[n+1]}$ yield the conditions on the complex
733 amplitudes

$$734 \quad \begin{Bmatrix} \mathbb{U}_1^{[n+1]} \\ \mathbb{U}_2^{[n+1]} \end{Bmatrix} = \mathbb{T}^{[n]} \cdot \begin{Bmatrix} \mathbb{U}_1^{[n]} \\ \mathbb{U}_2^{[n]} \end{Bmatrix}, \quad (\text{C.2})$$

735 where the transfer matrix $\mathbb{T}^{[n]}$ reads

$$736 \quad \mathbb{T}^{[n]} = \frac{1}{2} \begin{bmatrix} (1 + z^{[n]})e^{ik^{[n]}\ell^{[n]}} & (1 - z^{[n]})e^{-ik^{[n]}\ell^{[n]}} \\ (1 - z^{[n]})e^{ik^{[n]}\ell^{[n]}} & (1 + z^{[n]})e^{-ik^{[n]}\ell^{[n]}} \end{bmatrix}. \quad (\text{C.3})$$

737 with impedance ratio $z^{[n]} = \rho^{[n]}c^{[n]}/\rho^{[n+1]}c^{[n+1]}$. Relation (C.2) yields

$$738 \quad \begin{Bmatrix} \mathbb{U}_1^{[\mathcal{N}+1]} \\ \mathbb{U}_2^{[\mathcal{N}+1]} \end{Bmatrix} = \mathbb{T} \cdot \begin{Bmatrix} \mathbb{U}_1^{[1]} \\ \mathbb{U}_2^{[1]} \end{Bmatrix}, \quad \mathbb{T} = \mathbb{T}^{[\mathcal{N}]} \cdot \dots \cdot \mathbb{T}^{[1]}. \quad (\text{C.4})$$

739 Then, the condition of quasi-periodicity with wavenumber k is prescribed in
 740 layers $\Omega^{[\mathcal{N}+1]}$ and $\Omega^{[1]}$,

$$741 \quad \begin{Bmatrix} \mathbb{U}_1^{[\mathcal{N}+1]} \\ \mathbb{U}_2^{[\mathcal{N}+1]} \end{Bmatrix} = \mathbb{T} \cdot \begin{Bmatrix} \mathbb{U}_1^{[1]} \\ \mathbb{U}_2^{[1]} \end{Bmatrix} = e^{ik\ell} \begin{Bmatrix} \mathbb{U}_1^{[1]} \\ \mathbb{U}_2^{[1]} \end{Bmatrix}, \quad (\text{C.5})$$

742 Equation (C.5) shows that $e^{ik\ell} = \text{eig}(\mathbb{T})$ is an eigenvalue $\text{eig}(\mathbb{T})$ of 2x2-matrix
 743 \mathbb{T} , which leads to the relation

$$744 \quad \det(\mathbb{T}) - \text{tr}(\mathbb{T})e^{ik\ell} + e^{2ik\ell} = 0. \quad (\text{C.6})$$

745 The wavenumber k takes the form, where ν is an integer:

$$746 \quad k = \left(\frac{1}{\ell} \text{Arg}(\text{eig}(\mathbb{T})) + 2\pi\nu \right) - i \left(\frac{1}{\ell} \text{Ln}(|\text{eig}(\mathbb{T})|) \right). \quad (\text{C.7})$$

747 Here, matrix \mathbb{T} and its eigenvalues depend on the frequency ω , and the cal-
 748 culated wavenumber k can be complex-valued. In the dual approach used
 749 in closing criterion based in Bloch-analysis, the wavenumber k can be pre-
 750 scribed, and the corresponding frequencies ω are found numerically by solving
 751 for ω in Eq. (C.6).

752 References

- 753 [1] H. Altenbach, G. A. Maugin, V. Erofeev (Eds.), Mechanics of General-
 754 ized Continua, Springer-Verlag Berlin Heidelberg, 2011.
- 755 [2] E. Cosserat, F. Cosserat, Théorie des corps déformables, Librairie Sci-
 756 entifique A. Hermann et Fils, Paris, 1909.
- 757 [3] P. Germain, The method of virtual power in continuum mechanics. part
 758 2: Microstructure, SIAM Journal on Applied Mathematics 25 (3) (1973)
 759 556–575.

- 760 [4] A. C. Eringen, *Microcontinuum Field Theories I. Foundations and*
761 *Solids*, Springer-Verlag, New York, 1999.
- 762 [5] A. C. Eringen, *Nonlocal Continuum Field Theories*, Springer-Verlag
763 *New York, Inc.*, 2002.
- 764 [6] R. Mindlin, Second gradient of strain and surface tension in linear elas-
765 ticity, *Int. J. Solids Structures* 1 (1965) 417–438.
- 766 [7] S. Forest, *Milieux continus généralisés et matériaux hétérogènes*, Presses
767 *de l'Ecole des Mines de Paris*, 2006.
- 768 [8] R. D. Mindlin, Micro-structure in linear elasticity, *Arch. Ration. Mech.*
769 *Anal.* 16 (1) (1964) 51–78.
- 770 [9] A. Berezovski, J. Engelbrecht, A. Salupere, K. Tamm, T. Peets, M. Bere-
771 zovski, Dispersive waves in microstructured solids, *International Journal*
772 *of Solids and Structures* 50 (2013) 1981–1990.
- 773 [10] A. Madeo, P. Neff, E. Aifantis, G. Barbagallo, M. V. D'agostino, On
774 the role of micro-inertia in enriched continuum mechanics, *Proceedings*
775 *of the Royal Society A* 473 (2017) 20160722,.
- 776 [11] A. Wautier, B. B.Guzina, On thesecond-order homogenization of wave
777 motion in periodic media and the sound of a chessboard, *Journal of the*
778 *Mechanics and Physics of Solids* 78 (2015) 382–414.
- 779 [12] I. V. Andrianov, V. I. Bolshakov, V. V. Danishevs'kyi, D. Weichert,
780 Higher order asymptotic homogenization and wave propagation in peri-
781 odic composite materials, *Proc. R. Soc. A* 464 (2008) 1181–1201.

- 782 [13] J. Fish, W. Chen, G. Nagai, Non-local dispersive model for wave prop-
783 agation in heterogeneous media: one-dimensional case, *Int. J. Numer.*
784 *Meth. Engng* 54 (2002) 331–346.
- 785 [14] R. Cornaggia, B. Guzina, Second-order homogenization of boundary and
786 transmission conditions for one-dimensional waves in periodic media,
787 *Int. J. Solids.Struct.* 188 (9) (2019) 88–102.
- 788 [15] A. Pichugin, H. Askes, A. Tyasb, Asymptotic equivalence of homogenisa-
789 tion procedures and fine-tuning of continuum theories, *Journal of Sound*
790 *and Vibration* 13 (2008) 858–874.
- 791 [16] D. D. Domenico, H. Askes, E. C. Aifantis, Gradient elasticity and disper-
792 sive wave propagation: Model motivation and length scale identification
793 procedures in concrete and composite laminates, *International Journal*
794 *of Solids and Structures* 158 (2019) 176–190.
- 795 [17] E. Sánchez-Palencia, *Non-homogeneous media and vibration theory*, Vol.
796 127 of *Lecture Notes in Physics*, Springer-Verlag, 1980.
- 797 [18] J.-L. Auriault, C. Boutin, C. Geindreau, *Homogenization of Coupled*
798 *Phenomena in Heterogenous Media*, ISTE, 2009.
- 799 [19] B. Gambin, E. Kröner, Higher-order terms in the homogenized stress-
800 strain relation of periodic elastic media, *Physica Status Solidi B: Basic*
801 *Solid State Physics* 151 (1989) 513–519.
- 802 [20] C. Boutin, J. L. Auriault, Rayleigh scattering in elastic composite mate-
803 rials, *International Journal of Engineering Science* 31 (12) (1993) 1669–
804 1689.

- 805 [21] C. Boutin, Microstructural effects in elastic composites, *Int. J. Solids*
806 *Structures* 33 (1996) 1023–1051.
- 807 [22] H. Askes, E. C. Aifantis, Gradient elasticity in statics and dynamics:
808 An overview of formulations, length scale identification procedures, fi-
809 nite element implementations and new results, *International Journal of*
810 *Solids and Structures* 48 (2011) 1962–1990.
- 811 [23] J. Yang, S. Guo, On using strain gradient theories in the analysis of
812 cracks, *International Journal of Fracture* 133 (2005) L19–L22.
- 813 [24] A. C. Eringen, On differential equations of non local elasticity and solu-
814 tions of screw dislocation and surface waves, *Journal of Applied Physics*
815 54 (1973) 4703.
- 816 [25] S. Forest, K. Sab, Stress gradient continuum theory, *Mechanics Research*
817 *Communications* 40 (2012) 16–25.
- 818 [26] K. Sab, F. Legoll, S. Forest., Stress gradient elasticity theory: existence
819 and uniqueness of solution, *Journal of Elasticity* 123 (2) (2016) 179–201.
- 820 [27] C. Polizzotto, Stress gradient versus strain gradient constitutive models
821 within elasticity, *International Journal of Solids and Structures* 51 (2014)
822 1809–1818.
- 823 [28] C. Polizzotto, A unifying variational framework for stress gradient
824 and strain gradient elasticity theories, *European Journal of Mechanics*
825 *A/Solids* 49 (2015) 430–440.

- 826 [29] S. Forest, K. Sab, Finite-deformation second-order micromorphic theory
827 and its relations to strain and stress gradient models, *Mathematics and*
828 *Mechanics of Solids* (2017) 1–21.
- 829 [30] R. J. LeVeque, *Numerical Methods for Conservation Laws*, Lectures in
830 *Mathematics*, Birkhäuser Verlag, Switzerland, 1992.
- 831 [31] L. Evans, *Partial Differential Equations*, Graduate Studies in Mathe-
832 *matics*, American Mathematical Society, 2010.
- 833 [32] E. Godlewski, P. Raviart, *Numerical Approximation of Hyperbolic Sys-*
834 *tems of Conservation Laws*, Springer-Verlag, 1996.
- 835 [33] A. Metrikine, On causality of the gradient elasticity models, *Journal of*
836 *Sound and Vibration* 297 (2006) 727–742.
- 837 [34] J. L. Auriault, G. Bonnet, Dynamique des composites élastiques
838 périodiques, *Archives of Mechanics* 37 (4-5) (1985) 269–284.
- 839 [35] J.-L. Auriault, C. Boutin, Long wavelength inner-resonance cut-off fre-
840 quencies in elastic composite materials, *International Journal of Solids*
841 *and Structures* 49 (2012) 3269–3281.
- 842 [36] E. Dontsov, R. Tokmashev, B. Guzina, A physical perspective of the
843 length scales in gradient elasticity through the prism of wave dispersion,
844 *Int. J. Solids and Structures* 50 (2013) 3674–3684.
- 845 [37] J. Lagarias, J. Reeds, M. Wright, P. Wright, Convergence properties of
846 the nelder-mead simplex method in low dimensions, *SIAM Journal of*
847 *Optimization* 9 (1) (1998) 112–147.

- 848 [38] T. Schwartzkopff, M. Dumbser, C. Munz, Fast high-order ader schemes
849 for linear hyperbolic equations, *J. Comput. Phys.* 197 (2) (2004) 532–
850 539.
- 851 [39] J. Piraux, B. Lombard, A new interface method for hyperbolic problems
852 with discontinuous coefficients: one-dimensional acoustic example, *J.*
853 *Comput. Phys.* 168 (1) (2001) 227–248.
- 854 [40] C. Bellis, B. Lombard, Simulating transient wave phenomena in acoustic
855 metamaterials using auxiliary fields, *Wave Motion* 86 (2019) 175–194.
- 856 [41] T. Schwartzkopff, M. Dumbser, C. Munz, Fast high-order ader schemes
857 for linear hyperbolic equations, *J. Comput. Phys.* 197 (2) (2004) 532–
858 539.